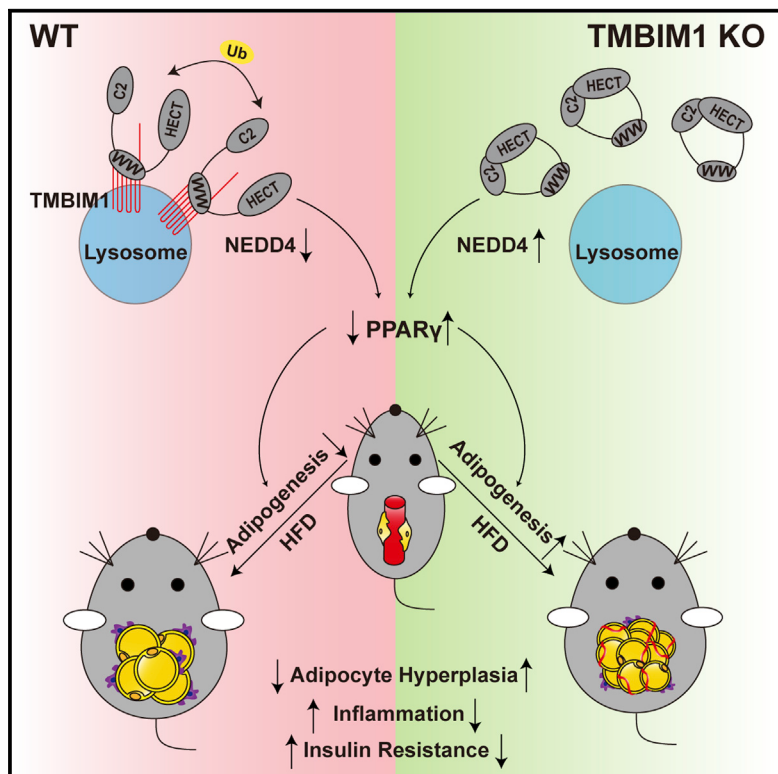


TMBIM1 is an inhibitor of adipogenesis and its depletion promotes adipocyte hyperplasia and improves obesity-related metabolic disease

Graphical abstract



Authors

Guang-Nian Zhao, Zheng-Wei Tian, Tian Tian, ..., Wenping Chen, Lan Bai, Hongliang Li

Correspondence

chenwenping@hgwy.org.cn (W.C.), bailan@whu.edu.cn (L.B.), lihl@whu.edu.cn (H.L.), yuanyf1971@whu.edu.cn (Y.Y.)

In brief

Zhao et al. identify TMBIM1, a lysosomal transmembrane protein, as an inhibitor of adipogenesis in adipocyte precursors both *in vitro* and *in vivo*, which acts by decreasing the stability of PPAR γ . In response to caloric excess, *Tmbim1* deletion in adipocyte precursors leads to hyperplastic visceral WAT expansion and improved obesity-related metabolic dysfunction.

Highlights

- A transcriptomic search identifies TMBIM1 as an inhibitor of adipogenesis
- *Tmbim1* KO in adipocyte precursors leads to hyperplastic EpiWAT expansion in obesity
- *Tmbim1* KO in adipocyte precursors leads to improved systemic metabolic health
- TMBIM1 inhibits adipogenesis by decreasing the stability of PPAR γ



Article

TMBIM1 is an inhibitor of adipogenesis and its depletion promotes adipocyte hyperplasia and improves obesity-related metabolic disease

Guang-Nian Zhao,^{1,2,8} Zheng-Wei Tian,^{1,2,8} Tian Tian,^{2,3,8} Zhi-Peng Zhu,^{1,2} Wen-Jie Zhao,^{1,2} Han Tian,² Xu Cheng,^{2,3} Feng-Jiao Hu,^{1,2} Man-Li Hu,^{1,2} Song Tian,² Ting Ding,^{4,5} Siping Chen,^{4,5} Yan-Xiao Ji,^{1,2} Peng Zhang,^{1,2} Xiao-Jing Zhang,^{1,2} Zhi-Gang She,^{2,3} Yufeng Yuan,^{6,7,*} Wenping Chen,^{4,5,*} Lan Bai,^{2,3,*} and Hongliang Li^{1,2,3,5,9,*}

¹Medical Science Research Center, Zhongnan Hospital, School of Basic Medical Sciences, Wuhan University, Wuhan, China

²Institute of Model Animal, Wuhan University, Wuhan, China

³Department of Cardiology, Renmin Hospital of Wuhan University, Wuhan, China

⁴Department of Endocrinology, Huanggang Central Hospital, Huanggang, China

⁵Huanggang Institute of Translational Medicine, Huanggang, China

⁶Department of Hepatobiliary & Pancreatic Surgery, Zhongnan Hospital of Wuhan University, Wuhan, China

⁷Clinical Medicine Research Center for Minimally Invasive Procedure of Hepatobiliary & Pancreatic Diseases of Hubei Province, Hubei, China

⁸These authors contributed equally

⁹Lead contact

*Correspondence: yuanyf1971@whu.edu.cn (Y.Y.), chenwenping@hggy.org.cn (W.C.), bailan@whu.edu.cn (L.B.), lihl@whu.edu.cn (H.L.)

<https://doi.org/10.1016/j.cmet.2021.05.014>

SUMMARY

Obesity is characterized by the excessive accumulation of the white adipose tissue (WAT), but healthy expansion of WAT via adipocyte hyperplasia can offset the negative metabolic effects of obesity. Thus, identification of novel adipogenesis regulators that promote hyperplasia may lead to effective therapies for obesity-induced metabolic disorders. Using transcriptomic approaches, we identified transmembrane BAX inhibitor motif-containing 1 (TMBIM1) as an inhibitor of adipogenesis. Gain or loss of function of TMBIM1 in preadipocytes inhibited or promoted adipogenesis, respectively. *In vivo*, in response to caloric excess, adipocyte precursor (AP)-specific *Tmbim1* knockout (KO) mice displayed WAT hyperplasia and improved systemic metabolic health, while overexpression of *Tmbim1* in transgenic mice showed the opposite effects. Moreover, mature adipocyte-specific *Tmbim1* KO did not affect WAT cellularity or nutrient homeostasis. Mechanistically, TMBIM1 binds to and promotes the autoubiquitination and degradation of NEDD4, which is an E3 ligase that stabilizes PPAR γ . Our data show that TMBIM1 is a potent repressor of adipogenesis and a potential therapeutic target for obesity-related metabolic disease.

INTRODUCTION

Obesity is characterized by excessive expansion of the white adipose tissue (WAT), and it is currently a major global public-health challenge, correlating strongly with cardiometabolic diseases, such as type 2 diabetes, dyslipidemia, and nonalcoholic fatty-liver disease (NAFLD) (Blüher, 2019; Cai et al., 2020). WAT is a critical regulator of systemic energy homeostasis as it synthesizes and stores triglycerides (TGs) for long-term energy needs, while liberating free fatty acids (FFAs) from TGs in times of energy demand. It also acts as an endocrine organ, secreting adipokines, such as leptin and adiponectin, that regulate whole-body metabolism (Rosen and Spiegelman, 2014). In response to overnutrition, WAT expands via an increase in the size of pre-existing adipocytes (i.e., hypertrophy) or through the generation of new adipocytes via the differentiation of adipocyte precursors (APs) during adipogenesis (i.e., hyperplasia). It is generally considered that hyperplasia of adipocytes is adaptive

and beneficial for metabolic health, whereas hypertrophy of adipocytes is maladaptive and associated with pathological WAT remodeling (Ghaben and Scherer, 2019; Vishvanath and Gupta, 2019).

Adipogenesis is a highly orchestrated process by which APs become committed to an adipogenic lineage (namely, preadipocytes), accumulate nutrients, and differentiate into mature adipocytes. Recent studies have suggested that the ability to recruit new adipocytes through adipogenesis is critical for both healthy adipose-tissue expansion and systemic metabolic health in the setting of caloric excess (Ghaben and Scherer, 2019; Vishvanath and Gupta, 2019). Emerging studies of mouse models have suggested that adipogenesis allows adipose tissue to expand while limiting hypoxia, inflammatory cell infiltration, and fibrosis, thus fully preserving the metabolic function of adipose tissue (Kusminski et al., 2012; Senol-Cosar et al., 2016; Shao et al., 2018). Therefore, the inability of WAT to expand through adipogenesis leads to a decline in WAT function, persistently elevated levels



of plasma glucose and lipids, and lipotoxicity in other metabolically sensitive organs, such as muscle, liver, and heart, which can promote insulin resistance. In addition, adipogenesis can vary between different fat depots. Studies in male mice utilizing different cell-tracking techniques have demonstrated that diet-induced obesity stimulates both hypertrophic and hyperplastic expansion of visceral epididymal WAT (EpiWAT), while subcutaneous inguinal WAT (IngWAT) grows only via hypertrophy (Jeffery et al., 2015; Shao et al., 2018; Wang et al., 2013).

In recent years, researchers have attempted to identify and characterize APs *in vivo* (Ferrero et al., 2020). APs reside within the vascular niche in adipose tissue, where they may sense systemic changes in metabolites and couple nutritional fluxes to adipogenesis (Berry et al., 2014; Cattaneo et al., 2020). One of the broadest markers of APs is platelet-derived growth-factor receptor α (PDGFR α), and the overwhelming majority of adult adipocytes are derived from this lineage (Berry and Rodeheffer, 2013; Cattaneo et al., 2020; Jeffery et al., 2014). Many of the regulatory mechanisms of adipogenesis have been elucidated using *in vitro* models of differentiation with preadipocyte cell lines. In response to differentiation stimuli, preadipocytes activate an adipogenic transcriptional cascade involving the nuclear hormone receptor PPAR γ , which is a master transcriptional regulator of adipogenesis and regulates essential aspects of adipose biology from development to metabolism (Gross et al., 2017; Letterova et al., 2014). The expression of PPAR γ has been shown to be regulated by various means, including by post-translational regulation. Several ubiquitin-protein E3 ligases that either degrade or stabilize PPAR γ have been identified in adipocytes (Kilroy et al., 2012; Kim et al., 2014; Li et al., 2016; Watanabe et al., 2015).

The strong correlation between adipogenesis and preserved metabolic health in obesity suggests that shifting adipose-tissue expansion from hypertrophy to hyperplasia could prevent pathological remodeling and adipose dysfunction in response to caloric excess. Therefore, the further identification of novel factors that modulate adipogenesis may improve our understanding of this process and may lead to the development of novel therapeutic approaches for the treatment of obesity-related metabolic disorders (Ghaben and Scherer, 2019; Vishvanath and Gupta, 2019). In this study, we leveraged transcriptomic data from mouse and human preadipocyte cell lines during adipocyte differentiation to identify potential regulators of adipogenesis. Among several candidates, TMBIM1 was selected for further study because of its prominent regulatory role in 3T3-L1 differentiation. Here, we applied functional genomic approaches both *in vitro* and *in vivo* to verify TMBIM1 as an inhibitor of adipogenesis, as a negative regulator of metabolically beneficial WAT plasticity and systemic nutrient homeostasis, and as a potential therapeutic target to promote improved metabolic health during overnutrition.

RESULTS

Identification of TMBIM1 as a regulator of adipogenesis

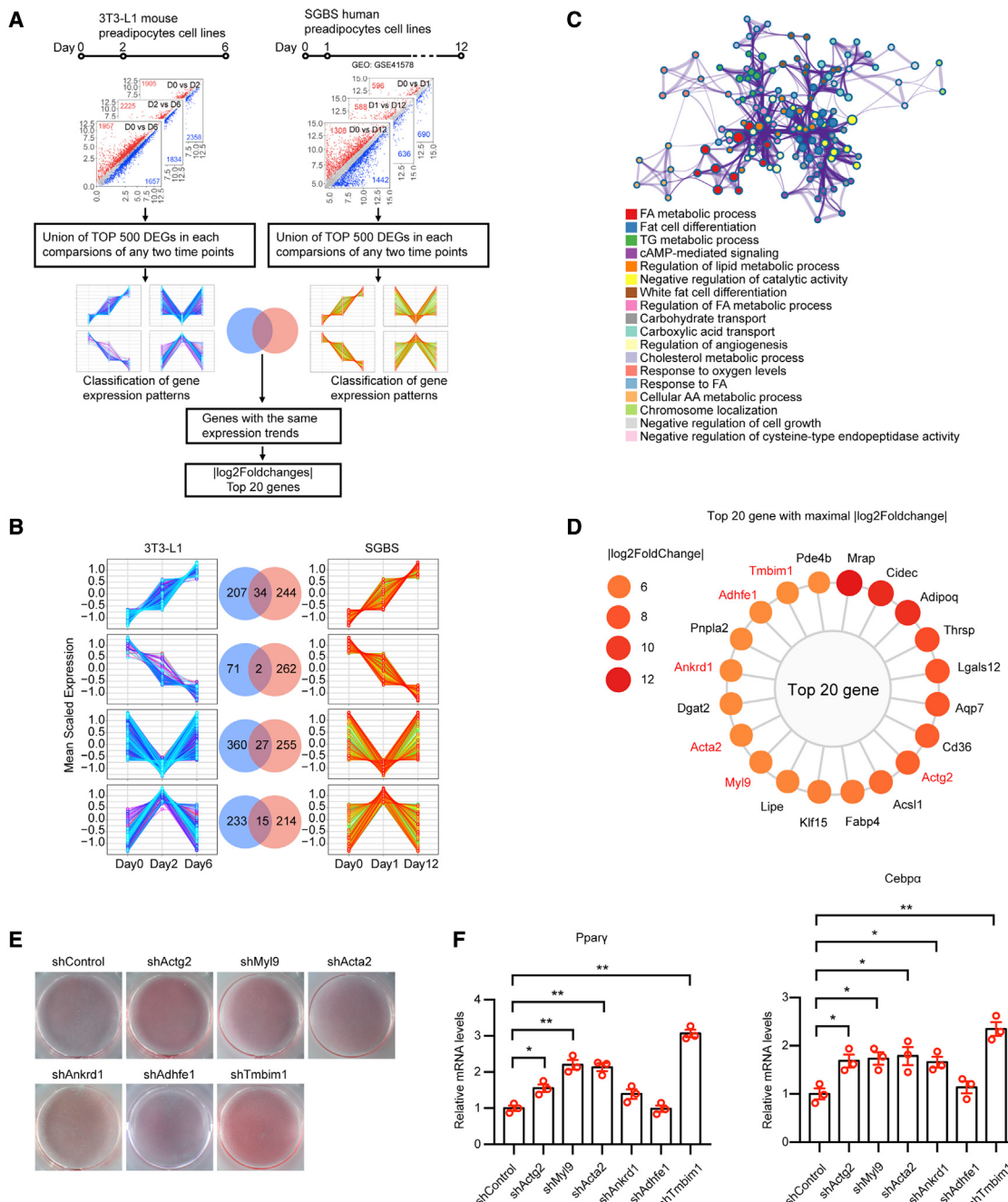
To identify potential key regulators associated with adipogenesis, we performed RNA sequencing (RNA-seq) analysis during 3T3-L1 adipocyte differentiation. RNA samples on days 0, 2, and 6 of differentiation were collected. We also reanalyzed pub-

licly available microarray data derived from the human preadipocyte Simpson-Golabi-Behmel syndrome (SGBS) cell line on days 0, 1, and 12 of differentiation (Galhardo et al., 2014) (Figures 1A and S1A). The top 500 differentially expressed genes (DEGs) based on fold change between any two of the three time points for each cell line were selected for further analysis. Expression-pattern classification revealed 78 genes with consistent trends during differentiation in the 3T3-L1 and SGBS cells (Figure 1B). Using functional enrichment analysis, we found that the functions of these genes were related to lipid metabolism and fat cell differentiation, demonstrating the effectiveness of this approach (Figure 1C). Among the top 20 DEGs, most of the identified genes, except for *Actg2*, *Myl9*, *Acta2*, *Ankrd1*, *Adhfe1*, and *Tmbim1*, have been reported to play a role during adipogenesis or in differentiated adipocytes (Figure 1D). To assess the involvement of these 6 genes in adipogenesis, we studied the effects of their loss of function in 3T3-L1 preadipocytes by knocking down their expression with lentiviruses encoding short-hairpin RNA and then inducing the adipogenic differentiation of the cells (Figure S1B). After 6 days of differentiation, Oil Red O staining and qPCR analysis showed that knockdown (KD) of *Tmbim1* among the 6 genes resulted in the most prominent effect compared with that of the control (Figures 1E and 1F).

Thereafter, we focused on TMBIM1 for further studies. We confirmed the expression of TMBIM1 during the differentiation of 3T3-L1 cells and mouse embryonic fibroblasts (MEFs). The qPCR and immunoblot analyses revealed that the mRNA and protein levels of TMBIM1 first decreased after induction and then increased during adipogenesis (Figures S1C–S1F). *Tmbim1* was similarly expressed in the APs and in mature adipocytes from the EpiWAT and IngWAT of mice, confirming that this protein has a potential role in APs (Figure S1G). We also measured TMBIM1 expression in a model of diet-induced obesity; the expression decreased in the EpiWAT and was not changed in the IngWAT of mice on a high-fat diet (HFD) compared with those on a normal chow diet (NCD) (Figures S1H and S1I).

TMBIM1 inhibits adipogenesis *in vitro*

We further confirmed the role of TMBIM1 in adipogenesis during 3T3-L1 differentiation after KD or overexpression of *Tmbim1* (Figures 2A and 2H). The adipocytes with *Tmbim1* KD accumulated higher levels of TGs than the control cells, as detected by BODIPY staining (Figure 2B). *Tmbim1* KD upregulated the mRNA and protein expression of PPAR γ and CEBP α during differentiation (Figures 2C and 2D). In contrast, overexpression of *Tmbim1* decreased the TG levels and reduced PPAR γ and CEBP α expression (Figures 2I–2K). To further evaluate the effects of TMBIM1 on adipogenesis, we assessed the samples on day 6 of induction after *Tmbim1* KD or overexpression by RNA-seq. After digital gene expression (DGE) analysis, we performed gene set enrichment analysis (GSEA) to identify the *Tmbim1* KD- or overexpression-specific gene-ontology biological process (GOBP) (Figures 2E and 2L). Notably, the results of GSEA showed that *Tmbim1* KD significantly upregulated—while *Tmbim1* overexpression significantly downregulated—lipid metabolism- and adipogenesis-related biological processes (Figures 2F and 2M). As shown in the heatmap, *Tmbim1* KD also significantly promoted the expression of genes involved in these biological

**Figure 1. Identification of TMBIM1 as a regulator of adipogenesis**

(A) Schematic illustration of the RNA-seq and bioinformatic analysis strategy.

(B) Dynamic change patterns of differentially expressed genes (DEGs) between each of the two consecutive stages. Different colors of line represent different genes. The number of genes with the same expression trends in 3T3-L1 and SGSB were indicated in the Venn diagram.

(C) Functional enrichment of genes with consistent expression trends in two cell lines.

(D) Top 20 genes based on the rank of maximal fold change absolute value.

(E) Oil Red O staining of adipocytes at day 6 of 3T3-L1 cell differentiation with indicated gene KD.

(F) qPCR analysis of mRNA expression of *Ppary* and *Cebpa* after KD of respective genes then induced adipogenic differentiation at day 6 in 3T3-L1 cells. Data are represented as mean \pm SEM. * p < 0.05, ** p < 0.01. Statistical analysis was carried out by Student's t test. See also Figure S1.

processes (Figure 2G). In contrast to the effect of *Tmbim1* KD, *Tmbim1* overexpression suppressed the genes related to lipid metabolism and adipogenesis (Figure 2N).

Differentiation of MEFs derived from the mice with global KO of *Tmbim1* was substantially promoted compared with that of the MEFs derived from the wild-type (WT) mice, as shown by the

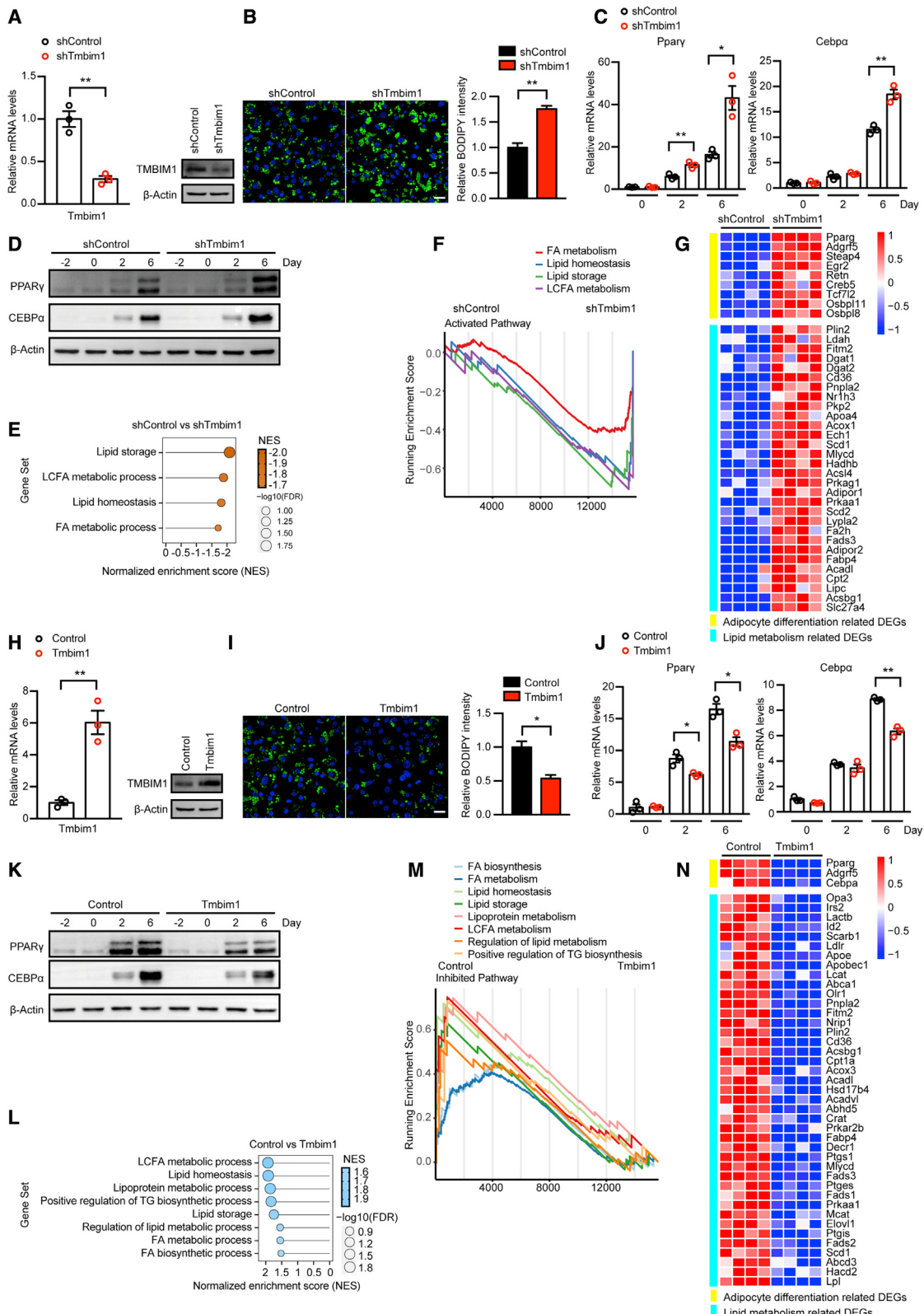


Figure 2. TMBIM1 inhibits adipogenesis *in vitro*

(A) TMBIM1 mRNA and protein expression in control and *Tmbim1* KD 3T3-L1 cells.

(B) BODIPY staining of adipocytes at day 6 of 3T3-L1 cell differentiation with *Tmbim1* KD. Scale bar, 20 μm.

Oil Red O staining and increased protein expression of PPAR γ and CEBP α after differentiation (Figures S2A and S2B). We further conducted RNA-seq analysis of the adipocytes differentiated from the WT and *Tmbim1* KO MEFs on day 6. Consistent with the inhibitory role of TMBIM1 in 3T3-L1 cells, GSEA of GOBP analysis and heatmap results revealed an enhancement of adipogenic biological processes and upregulation of gene expression related to adipocyte differentiation and lipid metabolism in the *Tmbim1* KO MEFs (Figures S2C and S2D). Additionally, we compared the *in vitro* differentiation of primary stromal vascular fractions (SVFs) isolated from both mouse genotypes. The *Tmbim1*-deficient IngWAT SVFs showed enhanced differentiation, as demonstrated by Oil Red O staining and increased adipogenic marker gene expression, after 6 days of differentiation, compared with the WT SVFs (Figures S2E–S2G). Overall, these *in vitro* data indicate that TMBIM1 inhibits adipogenesis.

***Tmbim1* deficiency in APs leads to hyperplastic EpiWAT expansion and improved systemic metabolic health**

To investigate the specific role of TMBIM1 in adipogenesis *in vivo*, we generated AP-specific KO mice using the *PdgfR α* Cre-lox system, which has been shown to be active in APs in lineage-tracing studies (Jeffery et al., 2014). This model has also been used in different studies to knockout genes in APs and in the adipocytes derived from them (Gao et al., 2020; Jeffery et al., 2015; Wagner et al., 2017). We bred mice carrying the floxed *Tmbim1* allele containing two loxP sites flanking exon 3 with transgenic mice expressing Cre recombinase driven by the *PdgfR α* promoter to generate *Tmbim1*-FloxB; *PdgfR α -Cre*^{+/-} mice (*Tmbim1*-APKO). Mice with the floxed *Tmbim1* alleles, which do not express Cre recombinase (*Tmbim1*-FloxB; *PdgfR α -Cre*^{-/-}), were used as controls, referred to hereafter as *Tmbim1*-FloxB mice. We enriched APs and Lin $^+$ (CD31 $^+$ CD45 $^+$ Ter119 $^+$) cells by bead purification and confirmed the specificity of cells isolated (Figure S3A). The full excision of the *Tmbim1* gene is achieved in APs from both EpiWAT and IngWAT, while Lin $^+$ cells still contain the full-length *Tmbim1* gene (Figure S3B). As expected, immunoblot analysis revealed a reduction in TMBIM1 expression in the EpiWAT and IngWAT of the *Tmbim1*-APKO mice

compared with the *Tmbim1*-FloxB mice, while there was no change in other tissues, verifying the specificity of the KO mice (Figure S3C).

To investigate the functional significance of AP-specific *Tmbim1* deletion, we fed both the *Tmbim1*-APKO and *Tmbim1*-FloxB mice an NCD or HFD for 12 weeks, starting at 8 weeks of age. During the 12-week period on either diet, the body weights of the *Tmbim1*-APKO mice remained indistinguishable from those of the *Tmbim1*-FloxB control animals (Figure S3D). Moreover, the WAT mass-to-body-weight ratio was the same in the NC *Tmbim1*-FloxB mice versus the *Tmbim1*-APKO mice, as was the HFD-induced increase in EpiWAT and IngWAT (Figure S3E). We did not detect any obvious histological differences in adipocyte size between the *Tmbim1*-APKO mice and the control animals fed an NCD (Figures 3A and S3F). However, consistent with the inhibitory role of TMBIM1 in adipogenesis, the EpiWAT from the HFD-fed mice had a greater adipocyte number than the controls, and these cells were smaller in size in the *Tmbim1*-APKO mice than in their control littermates, indicating the development of hyperplastic obesity (Figure 3A). However, the adipocyte size of the IngWAT was not changed (Figure S3F).

Next, we assessed glucose homeostasis in the NCD- and HFD-fed *Tmbim1*-FloxB and *Tmbim1*-APKO mice. No changes in fasting glucose, glucose, or insulin tolerance were observed in the lean NC-fed mice between genotypes (Figures 3B, 3D, and 3E). In contrast, on the HFD, the fasting blood-glucose and insulin levels were lower in the *Tmbim1*-APKO mice (Figures 3B and 3C). Moreover, the HFD-fed *Tmbim1*-APKO mice showed improved glucose and insulin tolerance compared with their *Tmbim1*-FloxB littermates (Figures 3D and 3E). Insulin-stimulated AKT phosphorylation was also significantly higher in the EpiWAT, but not changed in the IngWAT, of the *Tmbim1*-APKO mice than that of the *Tmbim1*-FloxB mice (Figures 3F and S3G). In the *Tmbim1*-APKO mice, the circulating levels of TGs and FFAs were lower than those of the control mice (Figures 3G and 3H). With respect to the adipokines, the *Tmbim1*-APKO mice exhibited lower leptin levels and higher adiponectin levels (Figures 3I and 3J). In addition, immunostaining for F4/80 clearly indicated that fewer macrophages were present in the EpiWAT of the *Tmbim1*-APKO mice than the *Tmbim1*-FloxB mice (Figure 3K).

- (C) *Ppar γ* and *Cebp α* mRNA levels during 3T3-L1 cell differentiation with *Tmbim1* KD.
- (D) PPAR γ and CEBP α protein levels during 3T3-L1 cell differentiation with *Tmbim1* KD.
- (E) Normalized enrichment scores (NES) of gene set enrichment analysis (GSEA) comparison of shControl and sh*Tmbim1*. A negative NES (orange) indicates that the gene set is associated with sh*Tmbim1*.
- (F) Enrichment plots of GSEA comparisons of shControl and sh*Tmbim1*. GSEA results shown are lipid metabolism- and adipogenesis-related GO biological processes differentially enriched in sh*Tmbim1*.
- (G) Heatmaps of the expression of leading genes from GSEA. Adipocyte differentiation and lipid-metabolism-related genes were upregulated (red) in sh*Tmbim1* (compared with shControl).
- (H) TMBIM1 mRNA and protein expression in control and *Tmbim1* overexpression 3T3-L1 cells.
- (I) BODIPY staining of adipocytes at day 6 of 3T3-L1 cell differentiation with *Tmbim1* overexpression. Scale bar, 20 μ m.
- (J) *Ppar γ* and *Cebp α* mRNA levels during 3T3-L1 cell differentiation with *Tmbim1* overexpression.
- (K) PPAR γ and CEBP α protein levels during 3T3-L1 cell differentiation with *Tmbim1* overexpression.
- (L) NES of GSEA comparison of control and *Tmbim1*. A positive NES (light blue) indicates that the gene set is associated with control.
- (M) Enrichment plots of GSEA comparison of control and *Tmbim1*. GSEA results shown are lipid metabolism- and adipogenesis-related GO biological processes differentially enriched in control.
- (N) Heatmaps of the expression of leading genes from GSEA. Adipocyte differentiation- and lipid metabolism-related genes were downregulated (blue) in *Tmbim1* (compared with control).

Data are represented as mean \pm SEM. *p < 0.05, **p < 0.01. Statistical analysis was carried out by Student's t test. See also Figure S2.

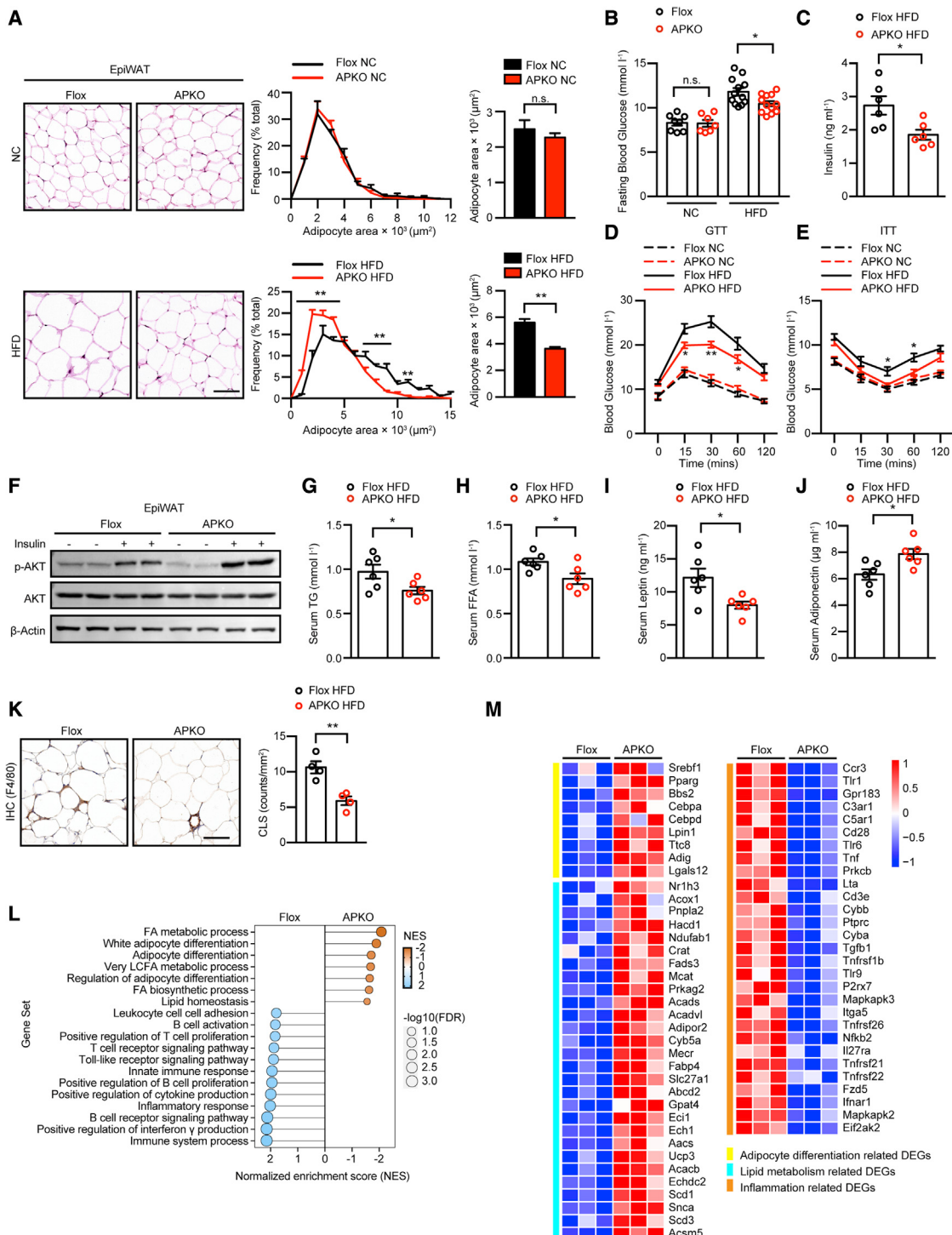


Figure 3. *Tmbim1* deficiency in APs leads to hyperplastic EpiWAT expansion and improved systemic metabolic health

(A) Hematoxylin and eosin (H&E) staining and adipocyte area of EpiWAT on NC or HFD. Scale bar, 100 μm .

(B) Fasting blood glucose levels after 12 weeks of NC or HFD feeding.

(C) Fasting serum insulin levels after 12 weeks of HFD feeding.

(D) Glucose tolerance tests (GTTs) after 10 weeks of NC or HFD feeding.

(E) Insulin tolerance test (ITT) after 11 weeks of NC or HFD feeding.

(F) Western blot analysis of insulin-stimulated phospho-Akt S473 (pS473AKT) in EpiWAT.

(G) Serum-TG levels after 12 weeks of HFD feeding.

(H) Serum-free fatty acid (FFA) levels after 12 weeks of HFD feeding.

(legend continued on next page)

We analyzed global gene expression in the EpiWAT samples from the *Tmbim1*-APKO mice and their control littermates by RNA-seq. Consistent with the enhanced adipogenesis, improved insulin sensitivity and fewer infiltrated macrophages were found in the EpiWAT of the *Tmbim1*-APKO mice compared with the control mice; GSEA of GOBP revealed enhanced adipocyte differentiation and repression of the inflammatory pathway (Figure 3L). Genes related to adipocyte differentiation and lipid metabolism were upregulated while genes related to inflammation were downregulated (Figure 3M). Taken together, these data demonstrate that obese *Tmbim1*-APKO mice exhibit a local adipose and systemic phenotype reminiscent of “insulin-sensitive” obesity.

***Tmbim1* overexpression in APs leads to pathological visceral WAT expansion and exacerbates metabolic dysfunction**

To further investigate the effects of the repressive function of AP *Tmbim1* in adipogenesis on metabolic homeostasis, we generated AP-specific *Tmbim1*-transgenic (*Tmbim1*-APTg) mice. Specific overexpression of *Tmbim1* in the EpiWAT and IngWAT was validated by immunoblotting (Figure S4A). We challenged control and *Tmbim1*-APTg animals with HFD feeding for a 12-week period. During the course of the HFD feeding, the body weights and overall adiposity of the *Tmbim1*-APTg mice again remained indistinguishable from those of the control animals (Figures S4B and S4C). The average size of the EpiWAT adipocytes was significantly larger in the *Tmbim1*-APTg mice than in the control mice, indicating increased adipocyte hypertrophy, which may reflect an attempt to compensate for the repressed adipogenesis in the EpiWAT of these animals (Figure 4A). However, the adipocyte size of IngWAT was not changed, similar to that in the *Tmbim1*-APKO mice (Figure S4D).

Consistent with the results from the *Tmbim1*-APKO mice, the fasting blood-glucose and insulin levels were higher in the *Tmbim1*-APTg mice than in the control mice (Figures 4B and 4C). After HFD feeding, the obese *Tmbim1*-APTg mice became relatively more glucose intolerant and insulin resistant than the obese controls (Figures 4D and 4E). Compared with that of the control animals, insulin-induced AKT phosphorylation was significantly impaired in the EpiWAT, but not altered in the IngWAT, of the *Tmbim1*-APTg mice (Figures 4F and S4E). Moreover, the levels of serum TGs and FFAs were relatively higher in the obese *Tmbim1*-APTg mice than in the controls (Figures 4G and 4H). And the levels of leptin and adiponectin were higher and lower, respectively, in the *Tmbim1*-APTg mice (Figures 4I and 4J). The EpiWAT of the *Tmbim1*-APTg mice exhibited robust

macrophage infiltrations, which suggested pathological adipose expansion (Figure 4K). Gene-expression analysis by qPCR revealed lower mRNA levels of the adipocyte-selective genes in the EpiWAT of the *Tmbim1*-APTg mice than in the controls, while the expression of genes related to inflammation was elevated (Figure 4L). Taken together, these data demonstrate that the impaired adipogenic capacity induced by AP *Tmbim1* overexpression results in pathological WAT expansion and exacerbates metabolic dysfunction.

Expression of TMBIM1 in mature adipocytes does not regulate adipogenesis and obesity-related metabolic dysfunction

To eliminate the possibility that TMBIM1 from mature adipocytes could affect adipogenesis, we generated inducible adipocyte-specific *Tmbim1* KO (designated *Tmbim1*-iAKO) mice by crossing *Tmbim1*-Flox mice with transgenic *Adipoq*-CreER mice, which express Cre recombinase under the control of the *Adipoq* promoter. Tamoxifen-induced recombination at 8 weeks of age led to mature adipocyte-specific *Tmbim1*-deficient mice. Genomic DNA analysis revealed that *Tmbim1* deletion occurred specifically in mature adipocytes but not in the SVFs of the EpiWAT and IngWAT (Figures S5A and S5B). Specific KO of *Tmbim1* in the EpiWAT and IngWAT was validated by immunoblotting (Figure S5C). Similar to the *Tmbim1*-APKO mice, the *Tmbim1*-iAKO mice showed unaltered body-weight growth curves and unaltered WAT depot weights during HFD feeding (Figures S5D and S5E). Importantly, however, the adipocyte size and number of the EpiWAT and IngWAT from the *Tmbim1*-iAKO mice were not altered compared with those of the control littermates, suggesting that TMBIM1 in mature adipocytes does not affect AP differentiation (Figures 5A and S5F). Consistent with the unchanged adipogenesis in the WAT of the *Tmbim1*-iAKO mice, the fasting blood-glucose levels were not changed compared with those in the control mice (Figure 5B). Moreover, the serum-insulin levels and insulin sensitivity of the *Tmbim1*-iAKO mice were the same as those of the control littermates (Figures 5C and 5D). Finally, the serum TG and FFA levels were also unaltered (Figures 5E and 5F). Taken together, these results indicate that expression of TMBIM1 in mature adipocytes does not affect HFD-induced adipocyte differentiation and systemic insulin resistance.

TMBIM1 decreases the stability of PPAR γ by promoting the degradation of NEDD4

To determine the mechanism underlying TMBIM1’s function during adipogenesis, we further analyzed the RNA-seq data obtained from 3T3-L1 cell induction with *Tmbim1* KD and

(I) Serum-leptin levels after 12 weeks of HFD feeding.

(J) Serum-adiponectin levels after 12 weeks of HFD feeding.

(K) F4/80 immuno-staining in EpiWAT and quantification of crown-like structures. Scale bar, 100 μ m.

(L) NES of GSEA comparison of Flox and *Tmbim1* APKO. A negative NES (orange) indicates that the gene set is associated with APKO. A positive NES (light blue) indicates that the gene set is associated with Flox.

(M) Heatmaps of the expression of leading genes from GSEA. Adipocyte differentiation and lipid-metabolism-related genes were upregulated (red) and inflammation related genes were downregulated (blue) in APKO, compared with Flox.

For (A), (B), (D), and (E), n = 8 Flox mice on NC; n = 7 APKO mice on NC; n = 12 Flox mice on HFD; n = 12 APKO mice on HFD. For (C) and (G)–(J), n = 6 mice per group. For (F), n = 4 mice for insulin injection per group. For (K), n = 4 mice per group. For (L) and (M), n = 3 mice per group. Data are represented as mean \pm SEM.

*p < 0.05, **p < 0.01. Statistical analysis: for (A), two-way ANOVA; for (B), (C), and (G)–(K), Student’s t test; for (D) and (E), two-way ANOVA with repeated measures. See also Figure S3.

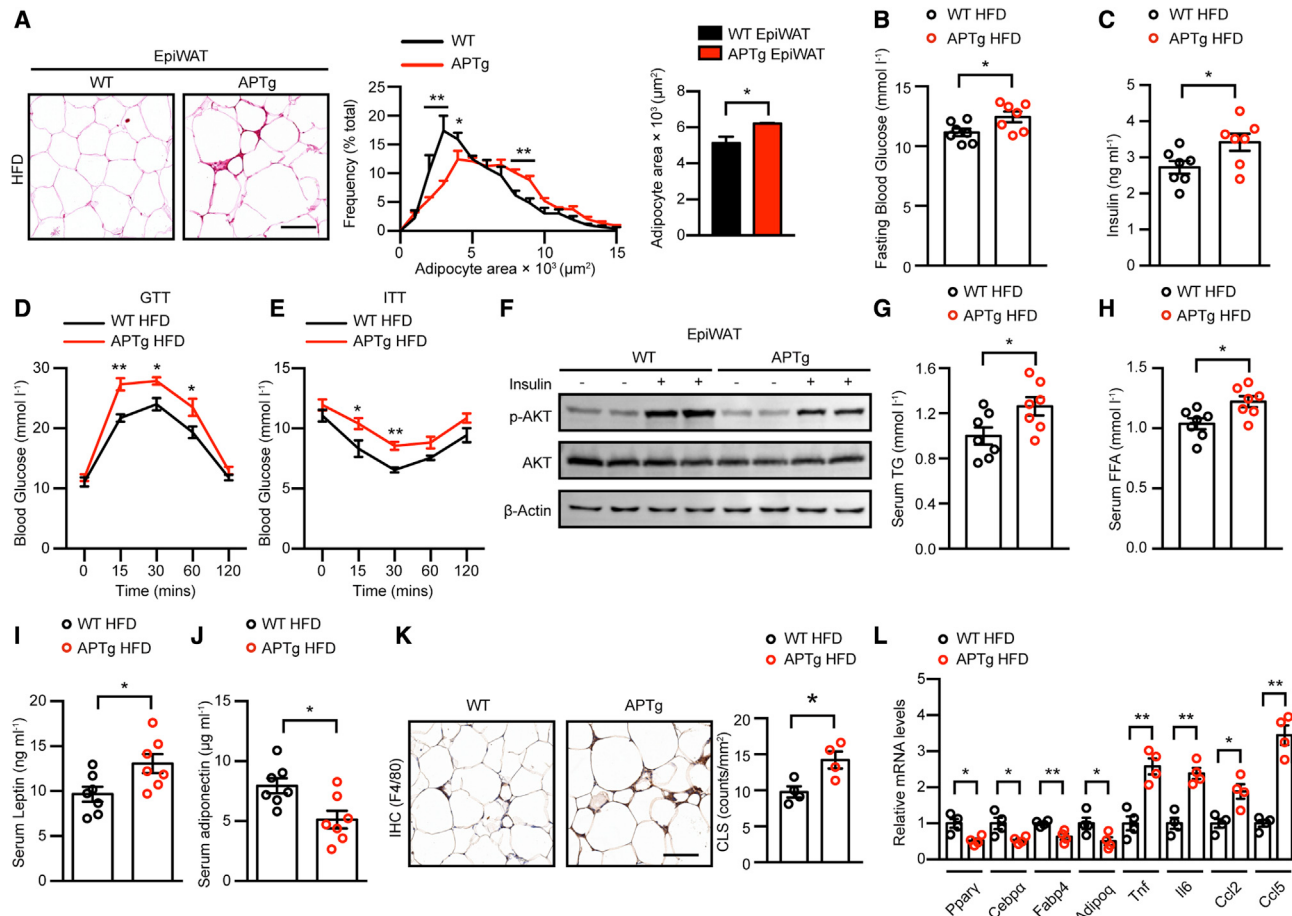


Figure 4. *Tmbim1* overexpression in APs leads to pathological visceral WAT expansion and exacerbates metabolic dysfunction

(A) H&E staining and adipocyte area of EpiWAT on HFD. Scale bar, 100 μm .

(B) Fasting blood glucose levels after 12 weeks of HFD feeding.

(C) Fasting serum insulin levels after 12 weeks of HFD feeding.

(D) GTT after 10 weeks of HFD feeding.

(E) ITT after 11 weeks of HFD feeding.

(F) Western blot analysis of insulin-stimulated pS473AKT in EpiWAT.

(G) Serum-TG levels after 12 weeks of HFD feeding.

(H) Serum-FFA levels after 12 weeks of HFD feeding.

(I) Serum-leptin levels after 12 weeks of HFD feeding.

(J) Serum-adiponectin levels after 12 weeks of HFD feeding.

(K) F4/80 immunostaining in EpiWAT and quantification of crown-like structures. Scale bar, 100 μm .

(L) qPCR of the indicated genes in EpiWAT after 12 weeks of HFD feeding.

For (A)–(E) and (G)–(J), n = 7 mice per group. For (F), n = 4 mice for insulin injection per group. For (K) and (L), n = 4 mice per group. Data are represented as mean \pm SEM. *p < 0.05, **p < 0.01. Statistical analysis: for (A), two-way ANOVA; for (B), (C), and (G)–(L), Student's t test; for (D) and (E), two-way ANOVA with repeated measures. See also Figure S4.

overexpression. A Kyoto Encyclopedia of Genes and Genomes (KEGG) pathway-enrichment analysis and GSEA based on KEGG pathways revealed that the most significant enrichments occurred in the PPAR signaling pathway (Figure 6A). As expected, only *Ppar γ* of the PPAR family exhibited altered expression (Figure 6B). Consistently, inhibition of protein translation using cycloheximide (CHX) revealed a significantly extended or reduced half-life of the PPAR γ protein levels in the 293T cells stably expressing hemagglutinin (HA)-tagged PPAR γ with *TMBIM1* KD or overexpression (Figure 6C). These results suggest that the inhibition of adipogenesis by TMBIM1 in 3T3-L1

cells was caused at least partially through the reduced stability of PPAR γ .

Our previous work demonstrated the function of TMBIM1 in the regulation of multivesicular body (MVB)-lysosome pathway, and lysosomal degradation of plasma-membrane proteins is dependent on the PSAP motif (amino acids 4–7) of TMBIM1 (Figure S6A) (Zhao et al., 2017). We asked whether the PSAP motif was required for the inhibitory effect of TMBIM1 on adipogenesis. Oil Red O staining showed the same degree of reduction in lipid accumulation in the 3T3-L1 cells overexpressing *Tmbim1* or *Tmbim1* with PSAP motif deletion and the control cells

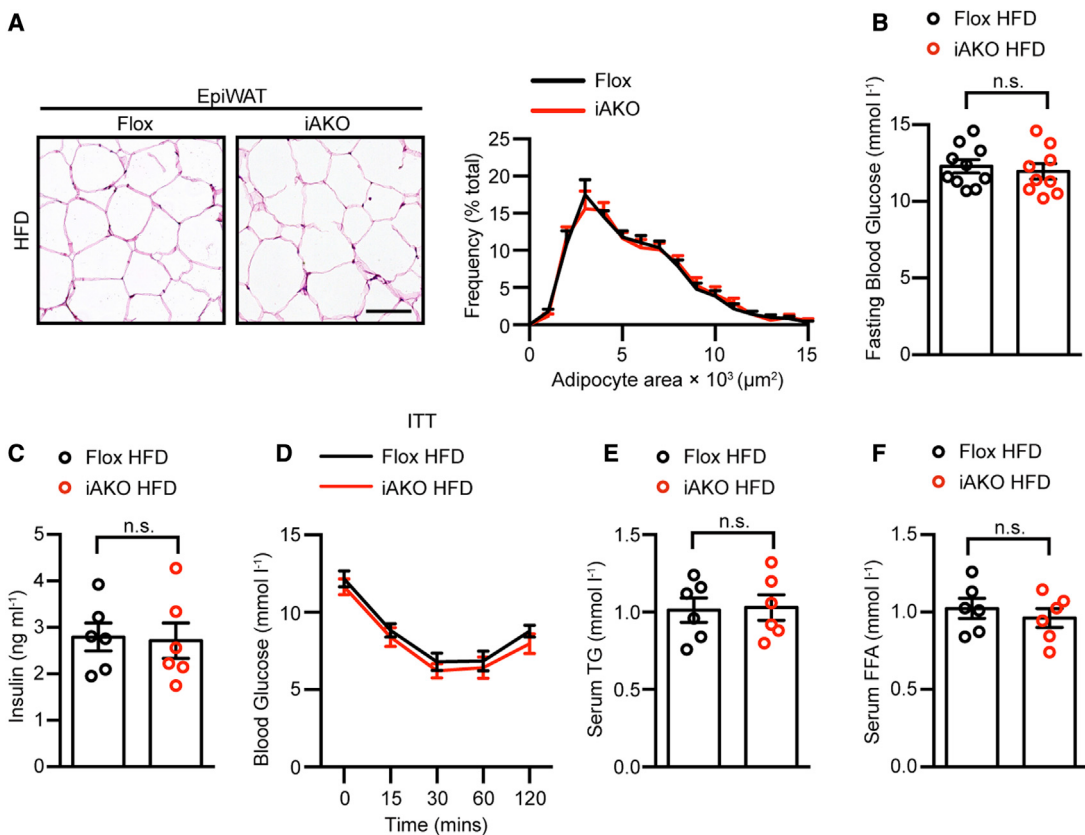


Figure 5. Expression of TMBIM1 in mature adipocytes does not regulate adipogenesis and obesity-related metabolic dysfunction

(A) H&E staining and adipocyte area of EpiWAT on HFD. Scale bar, 100 μm.

(B) Fasting blood glucose levels after 12 weeks of HFD feeding.

(C) Fasting serum insulin levels after 12 weeks of HFD feeding.

(D) ITT after 11 weeks of HFD feeding.

(E) Serum-TG levels after 12 weeks of HFD feeding.

(F) Serum-FFA levels after 12 weeks of HFD feeding.

For (A), (B), and (D), n = 10 Flox mice; n = 9 iAKO mice. For (C), (E), and (F), n = 6 mice per group. Data are represented as mean ± SEM. n.s., not significant. Statistical analysis was carried out by Student's t test. See also Figure S5.

(Figures S6B and S6C). RNA-seq analysis also revealed that the suppression of PPAR signaling and the lipid metabolic pathway conferred by TMBIM1 with PSAP motif deletion was comparable with that conferred by full-length TMBIM1 (Figures S6D and S6E). These results demonstrated that the PSAP motif and the corresponding regulatory effect of TMBIM1 on the MVB-lysosome pathway were not required for TMBIM1's role in adipogenic inhibition. Consistently, MG132, a proteasome inhibitor, but not chloroquine, a lysosome inhibitor, reversed the destabilization of PPAR γ conferred by TMBIM1, which further confirmed the well-established proteasome-dependent degradation of PPAR γ (Figure 6D).

We next examined the potential interaction between TMBIM1 and PPAR γ but obtained a negative result (Figure 6E). As TMBIM1 affects the stability of PPAR γ and no direct interaction exists between them, we hypothesized that there may be a regulator controlling the stability of PPAR γ that is controlled by TMBIM1. Next, we performed a comprehensive interactomic analysis of TMBIM1 in differentiated adipocytes and found multiple protein interactions, among which NEEDD4 is the only known

E3 ligase of PPAR γ (Figure 6F; Table S1). FLAG-tagged TMBIM1 could be immunoprecipitated with endogenous NEEDD4 in adipocytes, and cellular colocalization of TMBIM1 and NEEDD4 was also observed (Figures 6G and S6F). Co-immunoprecipitation analysis confirmed that the WW domains of NEEDD4 mediate the interaction between these two proteins (Figures S6A and S6G). Unexpectedly, however, both the cytoplasmic component and transmembrane domain of TMBIM1 could interact with NEEDD4 (Figures S6A and S6H). NEEDD4 can interact with PPAR γ to promote its stability by inhibiting its degradation and repress adipocyte differentiation in 3T3-L1 cells, as previously reported (Figures S6I and S6J) (Li et al., 2016). TMBIM1 reduced the half-life of the NEEDD4 protein in the presence of CHX, suggesting that TMBIM1 promotes the degradation of NEEDD4 (Figure 6H). TMBIM1 also negatively regulated the expression of NEEDD4 during 3T3-L1 adipocyte differentiation (Figure S6K). Consistently, NEEDD4 and PPAR γ expression in the SVFs isolated from EpiWAT was higher in the *Tmbim1*-APKO mice than in the control littermates after HFD feeding (Figure 6I). In addition, NEEDD4 and PPAR γ expression in the EpiWAT were also higher or lower

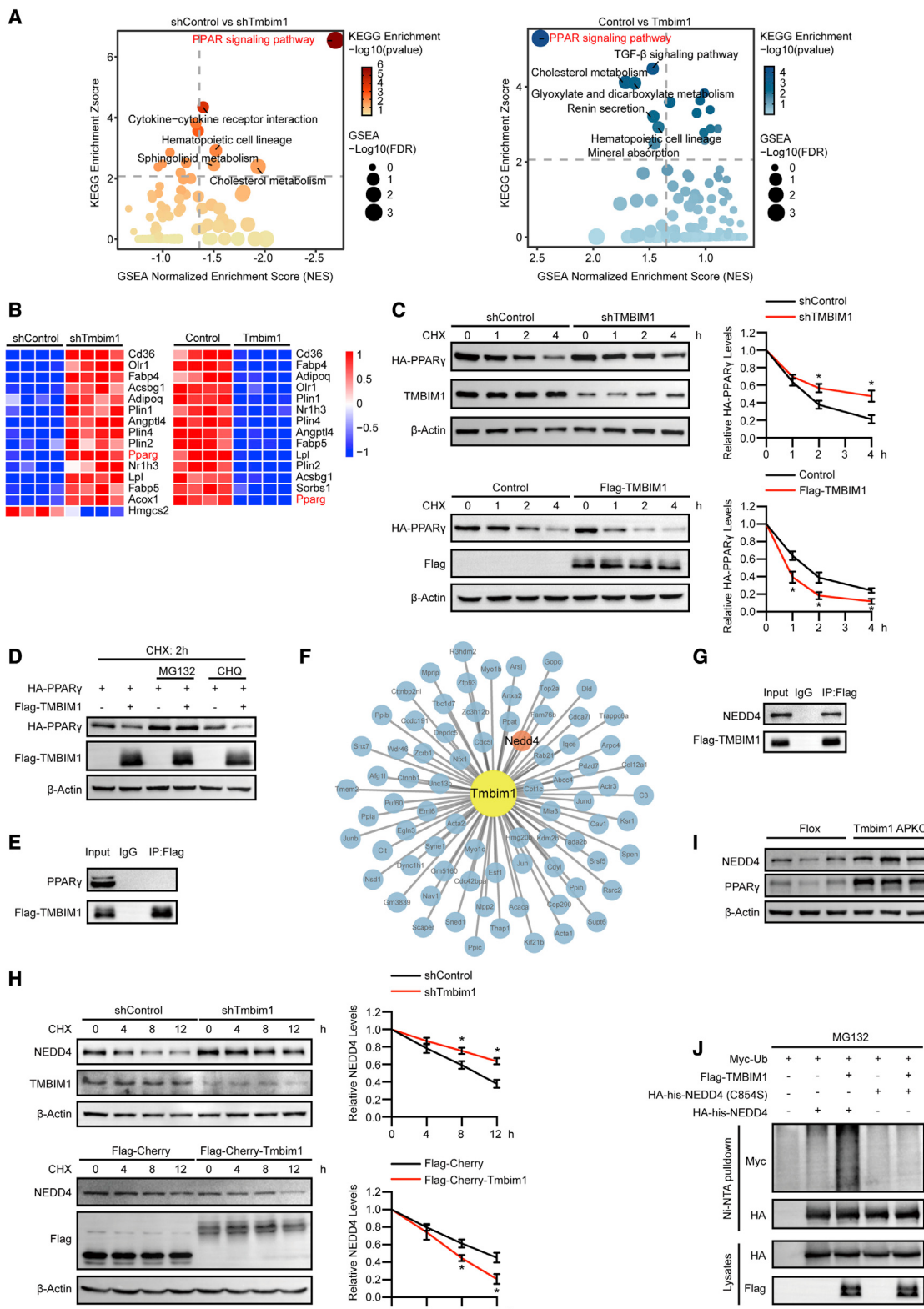


Figure 6. TMBIM1 decreases the stability of PPAR γ by promoting the degradation of NEDD4

(A) Pathways significantly enriched in KEGG pathway enrichment analysis of DEGs and GSEA based on KEGG pathway. The picture on the left shows there are five pathways enriched ($p < 0.05$, FDR < 0.25) in the comparison between shControl and shTmbim1. The picture on the right shows that there are seven pathways enriched ($p < 0.05$, FDR < 0.25) in the comparison between control and Tmbim1. In both comparisons, PPAR signaling is the most significantly enriched pathway.

(legend continued on next page)

in the *Tmbim1*-APKO mice or in the *Tmbim1*-APTg mice, respectively, compared with the control mice (Figure S6L). Stimulated degradation of NEDD4 can result from its increased catalytic activity, which can be monitored by an increase in its autoubiquitination. Consistent with the role of TMBIM1 in promoting the degradation of NEDD4, TMBIM1 enhanced the autoubiquitination of NEDD4, which required the catalytic activity of NEDD4 (Figure 6J). Finally, KD of *Nedd4* partially reversed lipid accumulation in *Tmbim1*-KD cells, as shown by Oil Red O staining (Figures S6M and S6N).

TMBIM1 inhibits adipogenesis via PPAR γ

We further asked whether the inhibitory role of TMBIM1 in adipogenesis was dependent on its regulation of PPAR γ . KD of *Ppar γ* substantially reversed lipid accumulation in the *Tmbim1*-KD cells, as shown by Oil Red O staining (Figures 7A and 7B). RNA-seq also revealed that the enhanced expression of genes related to adipocyte differentiation and lipid metabolic processes in the *Tmbim1* KD cells were reversed by *Ppar γ* KD (Figure 7C). To further confirm TMBIM1 regulation of adipogenesis via PPAR γ *in vivo*, we generated *Tmbim1*/*Ppar γ* AP-specific double KO (DKO) mice by crossing *Tmbim1*-Flox/*Ppar γ* -Flox mice with *PdgfRa*-cre mice. However, these DKO mice showed lipodystrophy with no detectable adipose tissue, which prevented further analysis. Therefore, we generated *Tmbim1*-Flox; *Ppar γ* -Flox/+; *PdgfRa*-cre mice (designated *Tmbim1*/*Ppar γ* ^{f/f} APKO) for the following study. The body weight and adiposity of the *Tmbim1*/*Ppar γ* ^{f/f} APKO mice were unaltered compared with those of the *Tmbim1*-Flox and *Tmbim1*-APKO mice (Figures S7A and S7B). Importantly, the adipocyte cellularity of the *Tmbim1*/*Ppar γ* ^{f/f} APKO mice, but not the small size of the adipocytes in the *Tmbim1*-APKO mice, was similar to that of the *Tmbim1*-Flox mice, suggesting that decreased expression of *Ppar γ* could reverse the enhanced adipogenesis of *Tmbim1* deficiency in APs (Figure 7D). Consistently, heterozygous *Ppar γ* reversed the improved glucose metabolic abnormalities and insulin resistance resulting from *Tmbim1* deficiency, as revealed by the fasting blood-glucose and insulin levels, glucose-tolerance tests, insulin-tolerance tests, and insulin-stimulated AKT activation in the EpiWAT (Figures 7E–7I). Taken together, these data suggest that the inhibitory effect of TMBIM1 on adipogenesis is largely dependent on PPAR γ .

DISCUSSION

The recruitment of new adipocytes in response to caloric excess through adipogenesis is regarded as a protective mechanism to ensure safe storage of energy in the WAT and prevent lipotoxicity in peripheral tissues, which is critical to the maintenance of systemic metabolic health (Ghaben and Scherer, 2019; Vishvanath and Gupta, 2019). Identification of novel regulators of adipogenesis may provide additional potential therapeutic molecular targets for the treatment of obesity-related metabolic disorders. Here, we demonstrate that TMBIM1 functions as a repressor of adipogenesis in APs, both *in vitro* and *in vivo*, by binding to and promoting the autoubiquitination and degradation of NEDD4, which is an E3 ligase that stabilizes PPAR γ .

TMBIM1 is a membrane protein that is located in MVB-lysosomes, and its expression is found to be upregulated in response to shear stress in endothelial cells (Yoshisue et al., 2002). TMBIM1 inhibits Fas-mediated apoptosis, maintains cellular Ca²⁺ homeostasis, and is involved in vascular diseases such as cystic medial degeneration (Lisak et al., 2015; Shukla et al., 2011; Zhao et al., 2006). Our previous studies have demonstrated a protective role for TMBIM1 in NAFLD and pathological cardiac hypertrophy (Deng et al., 2018; Zhao et al., 2017). In stressed hepatocytes and cardiomyocytes, TMBIM1 promotes the biogenesis of MVBs and accelerates the lysosomal degradation of activated Toll-like receptor 4, which is a pattern recognition receptor that activates inflammatory responses. In this work, TMBIM1 stands out as a prominent regulator of adipogenesis in our unbiased systematic transcriptomic analysis, so we continued to further study its function and underlying mechanism in APs. Unlike its inflammation repressive roles in hepatocytes and cardiomyocytes, the primary function of TMBIM1 in APs is inhibition of adipogenesis. And the repressive role of TMBIM1 in adipogenesis is unexpectedly not dependent on its function in the MVB-lysosome pathway, as the deletion of PSAP motif, which is essential for regulation of the MVB formation by TMBIM1, does not abolish its inhibitory effect in 3T3-L1 adipocyte differentiation. Instead, TMBIM1 indirectly reduces the stability of PPAR γ by interacting with and promoting the degradation of NEDD4. Accordingly, while TMBIM1 in hepatocytes attenuates NAFLD and metabolic disorders by repressing inflammation, TMBIM1 in APs aggravates pathological WAT remodeling and metabolic dysfunctions by inhibiting

- (B) The expression of DEGs enriched in PPAR signaling pathway. Left, shControl and shTmbim1; right, control and *Tmbim1*.
 - (C) Effect of TMBIM1 on the stability of PPAR γ 2. Treatment of 293T cells stably expressing HA-PPAR γ 2 with TMBIM1 KD or overexpression using CHX (100 μ M) for the indicated time. The indicated proteins were measured by immunoblotting and quantified.
 - (D) Effects of MG132 or chloroquine on TMBIM1-mediated PPAR γ 2 degradation. 293T cells stably expressing HA-PPAR γ 2, transfected with the TMBIM1 plasmids as indicated above, were treated with MG132 (10 μ M) or chloroquine (50 μ M) in the presence of CHX (100 μ M) for 2 h. The indicated proteins were measured by immunoblotting.
 - (E) Co-immunoprecipitation of TMBIM1 with PPAR γ in 3T3-L1 adipocytes.
 - (F) Interacting proteins of TMBIM1 (yellow) identified in interactomic. The orange dot is the only E3 ligase of these proteins, that is, NEDD4.
 - (G) Co-immunoprecipitation of TMBIM1 with NEDD4 in 3T3-L1 adipocytes.
 - (H) Effect of TMBIM1 on the stability of NEDD4. Treatment of 3T3-L1 cells with *Tmbim1* KD or overexpression using CHX (100 μ M) for the indicated time. The indicated proteins were measured by immunoblotting and quantified.
 - (I) Immunoblotting of NEDD4 and PPAR γ in isolated SVFs from EpiWAT of *Tmbim1*-APKO and control mice fed on HFD for 4 weeks.
 - (J) Effect of TMBIM1 on the auto-ubiquitination of NEDD4. 293T cells were transfected with the indicated plasmids for 24 h, for the last 6 h in the presence of MG132 (10 μ M). Cell lysates and pull-down of his-tagged NEDD4 were immunoblotted with the indicated antibodies.
- For (C) and (H), n = 3 independent experiments. Data are represented as mean \pm SEM. *p < 0.05, statistical analysis was carried out by Student's t test. See also Figure S6 and Table S1

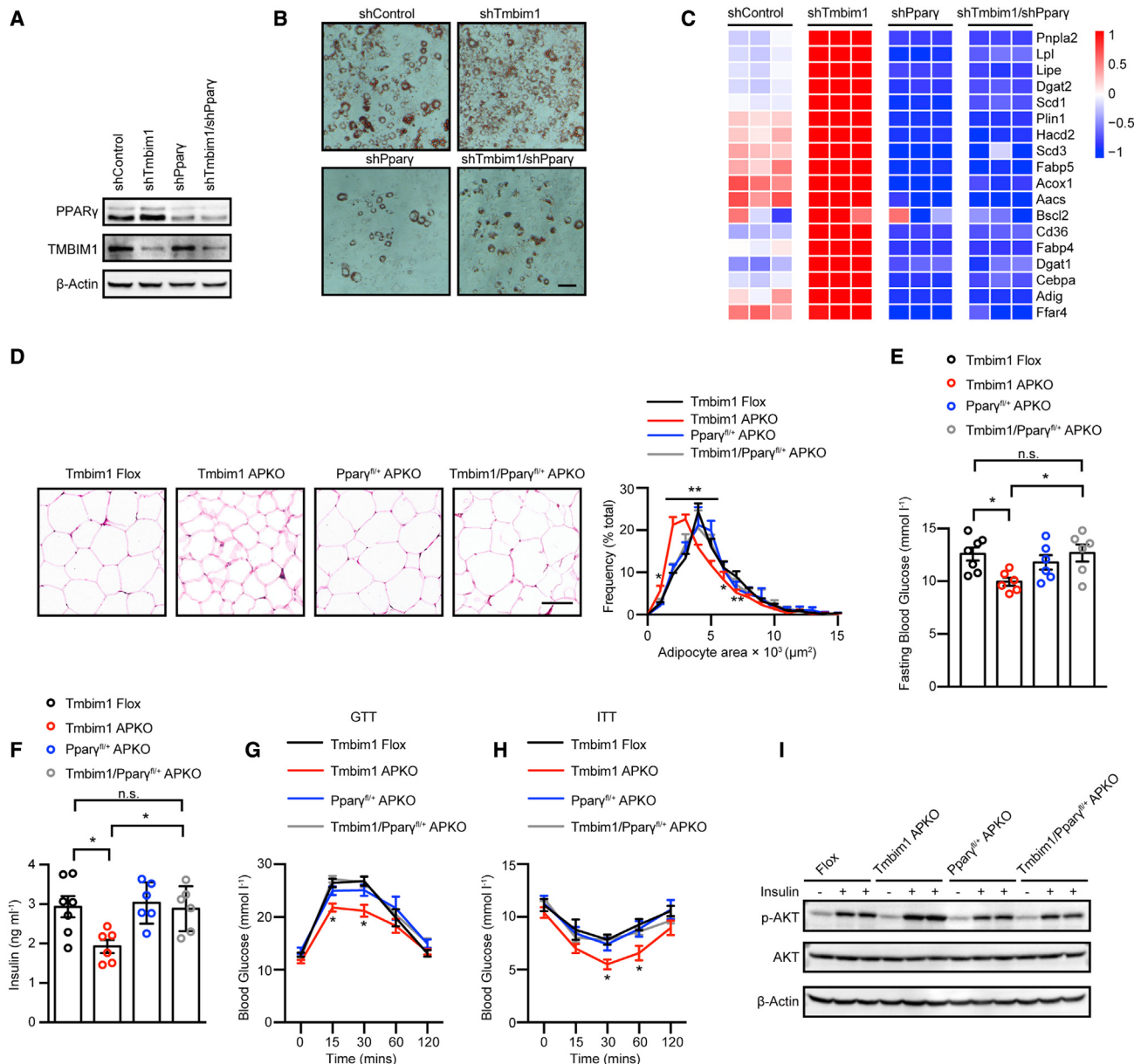


Figure 7. TMBIM1 inhibits adipogenesis via PPAR γ .

- (A) PPAR γ and TMBIM1 protein levels in adipocytes at day 6 of 3T3-L1 cell differentiation.
- (B) Oil Red O staining of adipocytes at day 6 of 3T3-L1 cell differentiation. Scale bar, 100 μm .
- (C) The heatmaps of the expression of lipid-metabolism-related genes at day 6 of 3T3-L1 cell differentiation (red, upregulated; blue, downregulated).
- (D) H&E staining and adipocyte area of EpiWAT on HFD. Scale bar, 100 μm .
- (E) Fasting blood glucose levels after 12 weeks of HFD feeding.
- (F) Fasting serum insulin levels after 12 weeks of HFD feeding.
- (G) GTT after 10 weeks of HFD feeding.
- (H) ITT after 11 weeks of HFD feeding.
- (I) Western blot analysis of insulin-stimulated pS473AKT in EpiWAT.

For (D)–(H), n = 7 *Tmbim1*-Flox mice; n = 6 *Tmbim1*-APKO mice; n = 6 *Ppar $\gamma^{fl/+}$* -APKO mice; n = 6 *Tmbim1/Ppar $\gamma^{fl/+}$* -APKO mice on HFD. For (I), n = 3 mice for insulin injection per group. Data are represented as mean \pm SEM. *p < 0.05, **p < 0.01. Statistical analysis: for (D), two-way ANOVA, *Tmbim1*-APKO group compared with *Tmbim1*-Flox group; for (E) and (F), one-way ANOVA; for (G) and (H), two-way ANOVA with repeated measures, *Tmbim1*-APKO group compared with *Tmbim1*-Flox group. See also Figure S7.

adipogenesis. Together, these results indicate that the multi-functional roles of TMBIM1 can be attributed to diverse molecular events regulated by TMBIM1 in cell-type-specific ways.

Furthermore, multiple therapeutic approaches might be developed by targeting the respective regulatory segments of TMBIM1 in different cell types and disease models.

In this study, various adipocyte differentiation and genetic mouse models were employed to validate TMBIM1 as a novel suppressor of adipogenesis. In preadipocyte cell lines or primary isolated MEFs and SVFs, TMBIM1 gain or loss of function inhibits or promotes adipocyte differentiation, respectively, which supports the cell-autonomous effects of TMBIM1 on adipogenesis. *In vivo*, TMBIM1 does not contribute significantly to the homeostatic replenishment of adipocytes in lean chow-fed mice, suggesting that TMBIM1 plays a negligible role in the developmental adipogenesis of WAT. In the setting of obesity, *Tmbim1* ablation in APs causes an increase in the number of adipocytes and an improvement in adipocyte function in EpiWAT, while the *Tmbim1* transgene has the opposite effects, which suggest TMBIM1 inhibits *de novo* adipogenesis in response to caloric excess. Moreover, our data indicate that expanding the number of visceral adipocytes can occur without increasing overall adiposity and body weight, even under increased caloric intake as previously reported (Shao et al., 2018). Notably, changes in adipose cellularity and sensitivity to insulin stimulation were restricted to EpiWAT but absent in IngWAT, which may be due to the few adipogenic events in IngWAT triggered by HFD feeding (Jeffery et al., 2015; Wang et al., 2013).

The systemic metabolic phenotypes in our AP KO and transgenic models are consistent with the concept that the health and functionality of the WAT determines systemic metabolic homeostasis (Ghaben and Scherer, 2019; Shao et al., 2018; Vishwanath and Gupta, 2019). Overall, adipogenesis now emerges as a viable therapeutic target and APs are gaining attention for their potential application in the clinic. A recent study provides evidence that antiadipogenic regulatory mechanisms within APs can be targeted pharmacologically as a means to stimulate adipogenesis and promote healthy WAT remodeling (Shao et al., 2021). Accordingly, it may be an attractive approach clinically to relieve the adipogenic capacity repressed by TMBIM1 in APs, which may improve WAT function and systemic metabolic health in obesity. In addition, the association between healthy WAT and metabolic health has largely been derived from studies of subcutaneous adipose tissue, while our data suggest that the health of visceral adipocytes also contributes, which is consistent with recent work (Senol-Cosar et al., 2016; Shao et al., 2018). Although adiponectin and leptin secreted by adipocytes may play a role, additional studies are needed to elucidate the precise mechanisms by which the health of visceral WAT can influence glucose homeostasis and insulin sensitivity. In addition, the contribution of *PdgfR α* -expressing perivascular cells present in other tissues cannot be excluded (Jeffery et al., 2014).

We propose that the decreased stability of PPAR γ is the primary molecular mechanism underlying the physiological function of TMBIM1 in adipogenesis. PPAR γ plays a central role in adipogenesis, and several E3 ligases have been reported to promote or reduce the proteasomal degradation of PPAR γ (Kilroy et al., 2012; Kim et al., 2014; Li et al., 2016; Watanabe et al., 2015). As TMBIM1 is an MVB- and lysosome-localized membrane protein while PPAR γ is a nuclear transcription factor, it is expected that no direct interaction exists between them. Thus, we speculated that an E3 ligase of PPAR γ may mediate the regulatory effect of TMBIM1 on PPAR γ . Our proteomic search for the binding protein of TMBIM1 in adipocytes revealed that the E3 ligase NEDD4 is such a target, which is of interest

given that it is known that NEDD4 can stabilize PPAR γ by preventing its proteasomal degradation (Li et al., 2016). NEDD4 contains a Ca $^{2+}$ -dependent, membrane-targeting C2 domain, followed by four WW domains that interact with particular proline-rich motifs and a C-terminal HECT domain that contains a catalytic cysteine residue (Huang et al., 2019). To prevent excessive ubiquitination of targets and self-destruction by autoubiquitination, HECT-type E3s normally adopt an inactive state characterized by intramolecular interactions (Zhu et al., 2017). We propose that TMBIM1 may function as an adaptor by binding to and releasing the autoinhibitory intramolecular interaction of NEDD4, and then, autoubiquitination of NEDD4 promotes its own degradation. In turn, this degradation of NEDD4 destabilizes PPAR γ , leading to an inhibition of adipogenesis.

In conclusion, our findings contribute to the current understanding of adipogenesis and identify new possibilities for the treatment of obesity-related metabolic disorders.

Limitations of study

It should be noted that our *Tmbim1* APKO is not an inducible KO model. As *Tmbim1* is constitutively manipulated in APs, mature adipocytes derived from these APs are also impacted. However, inducible KO of *Tmbim1* in mature adipocytes does not affect the size and function of adipocytes or systemic metabolic health, which strongly suggests that the phenotype in *Tmbim1*-APKO mice is due to the function of TMBIM1 in APs. To more specifically define the inhibitory role of TMBIM1 in APs in the context of adult animals, the recently confirmed inducible AP Cre mice are needed in future studies (Cattaneo et al., 2020; Shao et al., 2018). Besides, although the WW domains of NEDD4 contribute to the interaction of TMBIM1 and NEDD4 as expected, we surprisingly find that both the cytoplasmic and transmembrane domains of TMBIM1 can bind to NEDD4. Therefore, additional analysis is needed to precisely identify the segments responsible for their interactions. In addition, during the course of the adipogenic program, APs are transformed into mature adipocytes with an adequate change in morphology. This requires a permissive cytoskeletal reorganization to accommodate the physical demands resulting from increased lipid accumulation. Although our preliminary data suggest some cytoskeleton genes, such as *Actg2*, *Acta2*, and *Myl9*, are involved in adipogenesis regulation, more detailed studies are needed to uncover their roles.

STAR★METHODS

Detailed methods are provided in the online version of this paper and include the following:

- KEY RESOURCES TABLE
- RESOURCE AVAILABILITY
 - Lead contact
 - Materials availability
 - Data and code availability
- EXPERIMENTAL MODEL AND SUBJECT DETAILS
 - Animals
 - Cell lines and treatment
 - Primary cell isolation
- METHOD DETAILS
 - Adipocyte differentiation

- Construction of the lentivirus vector
- Plasmid construction
- RNA isolation and qPCR
- Western blotting
- Histological analyses and adipocyte size
- Immunoprecipitation assay
- *In vivo* ubiquitination assays
- Cellular localization
- RNA-Seq
- Digital gene expression
- Microarray data analysis
- Gene expression patterns classification
- Functional enrichment
- KEGG pathway enrichment analysis
- Gene set enrichment analysis
- Gene set variation analysis
- Mass spectrometry analysis

● QUANTIFICATION AND STATISTICAL ANALYSIS

SUPPLEMENTAL INFORMATION

Supplemental information can be found online at <https://doi.org/10.1016/j.cmet.2021.05.014>.

ACKNOWLEDGMENTS

This work was supported by grants from National Key R&D Program of China (2016YFF0101504 to Z.-G.S. and 2020YFC2004702 to Y.Y.), the National Science Foundation of China (81630011 to H.L., 81970364 and 81770053 to Z.-G.S., 81970070 to X.-J.Z., 81970011 to P.Z., 81700356 to Y.-X.J., and 82000600 to F.-J.H.), the Hubei Science and Technology Support Project (2019BFC582 and 2018BEC473 to H.L.), Hubei Provincial Natural Science Foundation of China (2018CFB137 to G.-N.Z.), Health Commission of Hubei Province scientific research project (WJ2021Q045 to G.-N.Z.), and Facilitate Scientific Research Special Funds of Henan Charity (GDXZ2021007 to G.-N.Z.).

AUTHOR CONTRIBUTIONS

G.-N.Z., Z.-W.T., and T.T. participated in research design; G.-N.Z., Z.-W.T., Z.-P.Z., W.-J.Z., H.T., F.-J.H., M.-L.H., and S.T. conducted experiments; G.-N.Z., Z.-W.T., T.T., and X.C. performed data analysis and interpretation; G.-N.Z. and T.T. drafted the paper; T.D., S.C., Y.-X.J., P.Z., X.-J.Z., and Z.-G.S. provided useful advice and edited the paper; Y.Y., W.C., L.B., and H.L. designed and supervised the studies; and all authors read and approved the final manuscript.

DECLARATION OF INTERESTS

The authors declare no competing interests.

Received: December 22, 2020

Revised: April 12, 2021

Accepted: May 13, 2021

Published: June 8, 2021

REFERENCES

- Berry, R., and Rodeheffer, M.S. (2013). Characterization of the adipocyte cellular lineage *in vivo*. *Nat. Cell Biol.* 15, 302–308.
- Berry, R., Jeffery, E., and Rodeheffer, M.S. (2014). Weighing in on adipocyte precursors. *Cell Metab.* 19, 8–20.
- Blüher, M. (2019). Obesity: global epidemiology and pathogenesis. *Nat. Rev. Endocrinol.* 15, 288–298.
- Cai, J., Zhang, X.J., Ji, Y.X., Zhang, P., She, Z.G., and Li, H. (2020). Nonalcoholic fatty liver disease pandemic fuels the upsurge in cardiovascular diseases. *Circ. Res.* 126, 679–704.
- Cattaneo, P., Mukherjee, D., Spinazzi, S., Zhang, L., Larcher, V., Stallcup, W.B., Kataoka, H., Chen, J., Dimmeler, S., Evans, S.M., and Guimarães-Camboa, N. (2020). Parallel lineage-tracing studies establish fibroblasts as the prevailing *in vivo* adipocyte progenitor. *Cell Rep.* 30, 571–582.e2.
- Church, C.D., Berry, R., and Rodeheffer, M.S. (2014). Isolation and study of adipocyte precursors. *Methods Enzymol.* 537, 31–46.
- Deng, K.-Q., Zhao, G.N., Wang, Z., Fang, J., Jiang, Z., Gong, J., Yan, F.-J., Zhu, X.-Y., Zhang, P., She, Z.-G., and Li, H. (2018). Targeting transmembrane BAX inhibitor motif containing 1 alleviates pathological cardiac hypertrophy. *Circulation* 137, 1486–1504.
- Ferrero, R., Rainer, P., and Deplancke, B. (2020). Toward a consensus view of mammalian adipocyte stem and progenitor cell heterogeneity. *Trends Cell Biol.* 30, 937–950.
- Galhardo, M., Sinkkonen, L., Berninger, P., Lin, J., Sauter, T., and Heinäniemi, M. (2014). Integrated analysis of transcript-level regulation of metabolism reveals disease-relevant nodes of the human metabolic network. *Nucleic Acids Res.* 42, 1474–1496.
- Gao, Z., Daquinag, A.C., Fussell, C., Zhao, Z., Dai, Y., Rivera, A., Snyder, B.E., Eckel-Mahan, K.L., and Kolonin, M.G. (2020). Age-associated telomere attrition in adipocyte progenitors predisposes to metabolic disease. *Nat. Metab.* 2, 1482–1497.
- Ghaben, A.L., and Scherer, P.E. (2019). Adipogenesis and metabolic health. *Nat. Rev. Mol. Cell Biol.* 20, 242–258.
- Gross, B., Pawlak, M., Lefebvre, P., and Staels, B. (2017). PPARs in obesity-induced T2DM, dyslipidaemia and NAFLD. *Nat. Rev. Endocrinol.* 13, 36–49.
- Hänzelmann, S., Castelo, R., and Guinney, J. (2013). GSVA: gene set variation analysis for microarray and RNA-seq data. *BMC Bioinformatics* 14, 7.
- Huang, X., Chen, J., Cao, W., Yang, L., Chen, Q., He, J., Yi, Q., Huang, H., Zhang, E., and Cai, Z. (2019). The many substrates and functions of NEDD4-1. *Cell Death Dis.* 10, 904.
- Jeffery, E., Berry, R., Church, C.D., Yu, S., Shook, B.A., Horsley, V., Rosen, E.D., and Rodeheffer, M.S. (2014). Characterization of Cre recombinase models for the study of adipose tissue. *Adipocyte* 3, 206–211.
- Jeffery, E., Church, C.D., Holtrup, B., Colman, L., and Rodeheffer, M.S. (2015). Rapid depot-specific activation of adipocyte precursor cells at the onset of obesity. *Nat. Cell Biol.* 17, 376–385.
- Jian, C., Fu, J., Cheng, X., Shen, L.-J., Ji, Y.-X., Wang, X., Pan, S., Tian, H., Tian, S., Liao, R., et al. (2020). Low-dose sorafenib acts as a mitochondrial uncoupler and ameliorates nonalcoholic steatohepatitis. *Cell Metab.* 31, 892–908.e811.
- Kilroy, G., Kirk-Ballard, H., Carter, L.E., and Floyd, Z.E. (2012). The ubiquitin ligase Siah2 regulates PPARgamma activity in adipocytes. *Endocrinology* 153, 1206–1218.
- Kim, J.H., Park, K.W., Lee, E.W., Jang, W.S., Seo, J., Shin, S., Hwang, K.A., and Song, J. (2014). Suppression of PPARgamma through MKRN1-mediated ubiquitination and degradation prevents adipocyte differentiation. *Cell Death Differ.* 21, 594–603.
- Kim, D., Paggi, J.M., Park, C., Bennett, C., and Salzberg, S.L. (2019). Graph-based genome alignment and genotyping with HISAT2 and HISAT-genotype. *Nat. Biotechnol.* 37, 907–915.
- Kusminski, C.M., Holland, W.L., Sun, K., Park, J., Spurgin, S.B., Lin, Y., Askew, G.R., Simcox, J.A., McClain, D.A., Li, C., and Scherer, P.E. (2012). MitoNEET-driven alterations in adipocyte mitochondrial activity reveal a crucial adaptive process that preserves insulin sensitivity in obesity. *Nat. Med.* 18, 1539–1549.
- Leferova, M.I., Haakonsson, A.K., Lazar, M.A., and Mandrup, S. (2014). PPARgamma and the global map of adipogenesis and beyond. *Trends Endocrinol. Metab.* 25, 293–302.
- Li, H., Handsaker, B., Wysoker, A., Fennell, T., Ruan, J., Homer, N., Marth, G., Abecasis, G., and Durbin, R.; 1000 Genome Project Data Processing Subgroup (2009). The Sequence Alignment/Map format and SAMtools. *Bioinformatics* 25, 2078–2079.

- Li, J.J., Wang, R., Lama, R., Wang, X., Floyd, Z.E., Park, E.A., and Liao, F.F. (2016). Ubiquitin ligase NEDD4 regulates PPARgamma stability and adipocyte differentiation in 3T3-L1 cells. *Sci. Rep.* 6, 38550.
- Lisak, D.A., Schacht, T., Enders, V., Habicht, J., Kiviluoto, S., Schneider, J., Henke, N., Bultyncik, G., and Methner, A. (2015). The transmembrane Bax inhibitor motif (TMBIM) containing protein family: tissue expression, intracellular localization and effects on the ER CA(2)(+)-filling state. *Biochim. Biophys. Acta* 1853, 2104–2114.
- Liu, D., Zhang, P., Zhou, J., Liao, R., Che, Y., Gao, M.M., Sun, J., Cai, J., Cheng, X., Huang, Y., et al. (2020). TNFAIP3 interacting protein 3 overexpression suppresses nonalcoholic steatohepatitis by blocking TAK1 activation. *Cell Metab.* 31, 726–740.e8.
- Love, M.I., Huber, W., and Anders, S. (2014). Moderated estimation of fold change and dispersion for RNA-seq data with DESeq2. *Genome Biol.* 15, 550.
- Lu, B., Klingbeil, O., Tarumoto, Y., Somerville, T.D.D., Huang, Y.H., Wei, Y., Wai, D.C., Low, J.K.K., Milazzo, J.P., Wu, X.S., et al. (2018). A transcription factor addiction in leukemia imposed by the MLL promoter sequence. *Cancer Cell* 34, 970–981.e8.
- Moffat, J., Grueneberg, D.A., Yang, X., Kim, S.Y., Kloepfer, A.M., Hinkle, G., Piqani, B., Eisenhaure, T.M., Luo, B., Grenier, J.K., et al. (2006). A lentiviral RNAi library for human and mouse genes applied to an arrayed viral high-content screen. *Cell* 124, 1283–1298.
- Parlee, S.D., Lentz, S.I., Mori, H., and MacDougald, O.A. (2014). Quantifying size and number of adipocytes in adipose tissue. *Methods Enzymol.* 537, 93–122.
- Pertea, M., Pertea, G.M., Antonescu, C.M., Chang, T.C., Mendell, J.T., and Salzberg, S.L. (2015). StringTie enables improved reconstruction of a transcriptome from RNA-seq reads. *Nat. Biotechnol.* 33, 290–295.
- Ritchie, M.E., Phipson, B., Wu, D., Hu, Y., Law, C.W., Shi, W., and Smyth, G.K. (2015). limma powers differential expression analyses for RNA-sequencing and microarray studies. *Nucleic Acids Res.* 43, e47.
- Rosen, E.D., and Spiegelman, B.M. (2014). What we talk about when we talk about fat. *Cell* 156, 20–44.
- Schneider, C.A., Rasband, W.S., and Eliceiri, K.W. (2012). NIH Image to ImageJ: 25 years of image analysis. *Nat. Methods* 9, 671–675.
- Senol-Cosar, O., Flach, R.J., DiStefano, M., Chawla, A., Nicoloro, S., Straubhaar, J., Hardy, O.T., Noh, H.L., Kim, J.K., Wabitsch, M., et al. (2016). Tenomodulin promotes human adipocyte differentiation and beneficial visceral adipose tissue expansion. *Nat. Commun.* 7, 10686.
- Shannon, P., Markiel, A., Ozier, O., Baliga, N.S., Wang, J.T., Ramage, D., Amin, N., Schwikowski, B., and Ideker, T. (2003). Cytoscape: a software environment for integrated models of biomolecular interaction networks. *Genome Res.* 13, 2498–2504.
- Shao, M., Vishvanath, L., Busbuso, N.C., Hepler, C., Shan, B., Sharma, A.X., Chen, S., Yu, X., An, Y.A., Zhu, Y., et al. (2018). De novo adipocyte differentiation from Pdgfr β + preadipocytes protects against pathologic visceral adipose expansion in obesity. *Nat. Commun.* 9, 890.
- Shao, M., Hepler, C., Zhang, Q., Shan, B., Vishvanath, L., Henry, G.H., Zhao, S., An, Y.A., Wu, Y., Strand, D.W., and Gupta, R.K. (2021). Pathologic HIF1 α signaling drives adipose progenitor dysfunction in obesity. *Cell Stem Cell* 28, 685–701.e7.
- Shukla, S., Fujita, K., Xiao, Q., Liao, Z., Garfield, S., and Srinivasula, S.M. (2011). A shear stress responsive gene product PP1201 protects against Fas-mediated apoptosis by reducing Fas expression on the cell surface. *Apoptosis* 16, 162–173.
- Subramanian, A., Tamayo, P., Mootha, V.K., Mukherjee, S., Ebert, B.L., Gillette, M.A., Paulovich, A., Pomeroy, S.L., Golub, T.R., Lander, E.S., and Mesirov, J.P. (2005). Gene set enrichment analysis: a knowledge-based approach for interpreting genome-wide expression profiles. *Proc. Natl. Acad. Sci. USA* 102, 15545–15550.
- Vishvanath, L., and Gupta, R.K. (2019). Contribution of adipogenesis to healthy adipose tissue expansion in obesity. *J. Clin. Invest.* 129, 4022–4031.
- Wagner, G., Lindroos-Christensen, J., Einwallner, E., Husa, J., Zapf, T.C., Lipp, K., Rauscher, S., Gröger, M., Spittler, A., Loewe, R., et al. (2017). HO-1 inhibits preadipocyte proliferation and differentiation at the onset of obesity via ROS dependent activation of Akt2. *Sci. Rep.* 7, 40881.
- Wang, Q.A., Tao, C., Gupta, R.K., and Scherer, P.E. (2013). Tracking adipogenesis during white adipose tissue development, expansion and regeneration. *Nat. Med.* 19, 1338–1344.
- Watanabe, M., Takahashi, H., Saeki, Y., Ozaki, T., Itoh, S., Suzuki, M., Mizushima, W., Tanaka, K., and Hatakeyama, S. (2015). The E3 ubiquitin ligase TRIM23 regulates adipocyte differentiation via stabilization of the adipogenic activator PPAR γ . *eLife* 4, e05615.
- Yoshisue, H., Suzuki, K., Kawabata, A., Ohya, T., Zhao, H., Sakurada, K., Taba, Y., Sasaguri, T., Sakai, N., Yamashita, S., et al. (2002). Large scale isolation of non-uniform shear stress-responsive genes from cultured human endothelial cells through the preparation of a subtracted cDNA library. *Atherosclerosis* 162, 323–334.
- Zhao, H., Ito, A., Kimura, S.H., Yabuta, N., Sakai, N., Ikawa, M., Okabe, M., Matsuzawa, Y., Yamashita, S., and Nojima, H. (2006). RECS1 deficiency in mice induces susceptibility to cystic medial degeneration. *Genes Genet. Syst.* 81, 41–50.
- Zhao, G.-N., Zhang, P., Gong, J., Zhang, X.-J., Wang, P.-X., Yin, M., Jiang, Z., Shen, L.-J., Ji, Y.-X., Tong, J., et al. (2017). Tmbim1 is a multivesicular body regulator that protects against non-alcoholic fatty liver disease in mice and monkeys by targeting the lysosomal degradation of Tir4. *Nat. Med.* 23, 742–752.
- Zhou, Y., Zhou, B., Pache, L., Chang, M., Khodabakhshi, A.H., Tanaseichuk, O., Benner, C., and Chanda, S.K. (2019). Metascape provides a biologist-oriented resource for the analysis of systems-level datasets. *Nat. Commun.* 10, 1523.
- Zhu, K., Shan, Z., Chen, X., Cai, Y., Cui, L., Yao, W., Wang, Z., Shi, P., Tian, C., Lou, J., et al. (2017). Allosteric auto-inhibition and activation of the Nedd4 family E3 ligase Itch. *EMBO Rep.* 18, 1618–1630.

STAR★METHODS

KEY RESOURCES TABLE

REAGENT or RESOURCE	SOURCE	IDENTIFIER
Antibodies		
Rabbit polyclonal anti-TMBIM1, dil: 1/1000	ABclonal	Cat#A8249; RRID: AB_2772628
Rabbit polyclonal anti-TMBIM1, dil: 1/1000	Sigma-Aldrich	Cat#HPA012093; RRID: AB_1858056
Mouse monoclonal anti-β-Actin, dil: 1/5000	Sigma-Aldrich	Cat#A5441; RRID: AB_476744
Rabbit monoclonal anti-GAPDH (clone D16H11), dil: 1/1000	Cell Signaling Technology	Cat#5174; RRID: AB_10622025
Rabbit monoclonal anti-PPAR γ (clone C26H12), dil: 1/1000	Cell Signaling Technology	Cat#2435; RRID: AB_2166051
Rabbit monoclonal anti-CEBP α (clone D56F10), dil: 1/1000	Cell Signaling Technology	Cat#8178; RRID: AB_11178517
Rabbit monoclonal anti-Phospho-AKT (Ser473) (clone D9E), dil: 1/1000	Cell Signaling Technology	Cat#4060; RRID: AB_2315049
Rabbit polyclonal anti-AKT, dil: 1/1000	Cell Signaling Technology	Cat#9272; RRID: AB_329827
Rabbit polyclonal anti-NEDD4, dil: 1/1000	Cell Signaling Technology	Cat#2740; RRID: AB_2149312
Rabbit monoclonal anti-HA-tag (clone C29F4), dil: 1/1000	Cell Signaling Technology	Cat#3724; RRID: AB_1549585
Mouse monoclonal anti-HA-tag, dil: 1/1000	MBL International	Cat#M180-3; RRID: AB_10951811
Mouse monoclonal anti-Flag-tag, dil: 1/1000	MBL International	Cat#M185-3L; RRID: AB_11123930
Mouse monoclonal anti-Myc-tag, dil: 1/1000	MBL International	Cat#M047-3; RRID: AB_591112
Rat monoclonal anti-F4/80, dil: 1/50	Bio-Rad	Cat#MCA497; RRID: AB_2098196
Goat anti-rabbit IgG-HRP, dil: 1/5000	Jackson ImmunoResearch Labs	Cat#111-035-003; RRID: AB_2313567
Goat anti-mouse IgG-HRP, dil: 1/5000	Jackson ImmunoResearch Labs	Cat#115-035-003; RRID: AB_10015289
Enhanced HRP goat anti-rat IgG polymer, dil: 1/50	ZSGB-Bio	Cat#PV-9004; RRID: AB_2868453
Clean-Blot IP Detection Reagent (HRP) antibody, dil: 1/500	Thermo Fisher Scientific	Cat#21230; RRID: AB_2864363
Normal mouse IgG, dil: 1/1000	Santa Cruz Biotechnology	Cat#sc-2025; RRID: AB_737182
Chemicals, peptides, and recombinant proteins		
Tamoxifen	Sigma-Aldrich	Cat#T5648; CAS: 10540-29-1
Corn oil	Aladdin	Cat#C116023
Insulin	Sigma-Aldrich	Cat#I6634; CAS: 11070-73-8
3-Isobutyl-1-methylxanthine (IBMX)	Sigma-Aldrich	Cat#I7018; CAS: 28822-58-4
Dexamethasone	Sigma-Aldrich	Cat#D4902; CAS: 50-02-2
Rosiglitazone	Sigma-Aldrich	Cat#R2408; CAS: 122320-73-4
Fetal Bovine Serum (FBS)	GIBCO	Cat#10099141C
New Born Calf Serum (NBCS)	Every Green	Cat#22011-8612
Polyethyleneimine	Polysciences	Cat#23966
Penicillin/Streptomycin	GIBCO	Cat#15140-122
Cycloheximide	Cell Signaling Technology	Cat#2112; CAS: 66-81-9
MG132	Beyotime	Cat#S1748; CAS: 133407-82-6
Chloroquine	Sigma-Aldrich	Cat#C6628; CAS: 50-63-5
Collagenase type II	Sigma-Aldrich	Cat#C6885; CAS: 9001-12-1
Formaldehyde solution	Sigma-Aldrich	Cat#F8775; CAS: 50-00-0
BODIPY 493/503	Thermo Fisher Scientific	Cat#D3922; CAS: 121207-31-6
Oil Red O	Sigma-Aldrich	Cat#O1391; CAS: 1320-06-5
DAPI	SouthernBiotech	Cat#0100-20

(Continued on next page)

Continued

REAGENT or RESOURCE	SOURCE	IDENTIFIER
TRI Reagent	Sigma-Aldrich	Cat#T9424
SYBR Green	Roche	Cat#04887352001
Protease inhibitor cocktail	Roche	Cat#04693132001
Phosphatase inhibitor	Roche	Cat#4906837001
Protein G-agarose	Roche	Cat#11719416001
Ni-NTA agarose	Qiagen	Cat#30210
Critical commercial assays		
ELISA Kit for Insulin	Cloud-Clone	Cat#CEA448Mu
ELISA Kit for Leptin	Cloud-Clone	Cat#SEA084Mu
ELISA Kit for Adiponectin	Cloud-Clone	Cat#SEA605Mu
Triglyceride (TG) assay kit	Wako	Cat#290-63701
FFA assay kit	Wako	Cat#294-63601
Adipose Tissue Progenitor Isolation Kit, mouse	Miltenyi Biotec	Cat#130-106-639
Transcriptor First Strand cDNA Synthesis Kit	Roche	Cat#04896866001
BCA Protein assay kit	Thermo Fisher Scientific	Cat#23225
3,3'-Diaminobenzidine (DAB) substrate kit	ZSGB-Bio	Cat#ZLI-9018
MGIEasy RNA Library Prep Kit	MGI Tech	Cat#1000006384
RNA 6000 Nano kit	Agilent	Cat#5067-1511
DNA 1000 Kit	Agilent	Cat#5067-1504
Deposited data		
RNA-seq data of 3T3-L1 cell adipocyte differentiation	This paper, NCBI SRA	SRA: PRJNA728240
RNA-seq data of adipocytes at day 6 of 3T3-L1 cell differentiation with <i>Tmbim1</i> knockdown/overexpression	This paper, NCBI SRA	SRA: PRJNA728494
RNA-seq data of adipocytes at day 6 of MEF differentiation from wild type and <i>Tmbim1</i> knockout mice	This paper, NCBI SRA	SRA: PRJNA728533
RNA-seq data of adipocytes at day 6 of 3T3-L1 cell differentiation with shControl, sh <i>Tmbim1</i> , sh <i>Pparγ</i> or sh <i>Tmbim1</i> /sh <i>Pparγ</i>	This paper, NCBI SRA	SRA: PRJNA728546
RNA-seq data of EpiWAT from <i>Tmbim1</i> -Flox and <i>Tmbim1</i> -APKO mice fed HFD for 12 weeks	This paper, NCBI SRA	SRA: PRJNA728526
RNA-seq data of adipocytes at day 6 of 3T3-L1 cell differentiation with Control, <i>Tmbim1</i> , <i>Tmbim1</i> ^{4PSAP} overexpression	This paper, NCBI SRA	SRA: PRJNA728551
Publicly available microarray datasets from SGBS adipocyte differentiation	GEO database	GEO: GSE41578
Experimental models: Cell lines		
Mouse: 3T3-L1	ATCC	Cat#CL-173
Human: HEK293T	Cell Bank of Type Culture Collection of the Chinese Academy of Sciences, Shanghai, China.	Cat#GNHu17
Experimental models: Organisms/strains		
Mouse: <i>Tmbim1</i> -flox mice	Zhao et al., 2017	N/A
Mouse: CAG-loxP-CAT-loxP- <i>Tmbim1</i> mice	Zhao et al., 2017	N/A
Mouse: C57BL/6-Tg(Pdgfra-cre)1Clc/J	The Jackson Laboratory	JAX: 013148
Mouse: B6.129- <i>Pparg</i> ^{tm2Rev} /J	The Jackson Laboratory	JAX: 004584

(Continued on next page)

Continued

REAGENT or RESOURCE	SOURCE	IDENTIFIER
Mouse: B6.129-Tg(Adipoq-cre/Esr1*)1Evdr/J	The Jackson Laboratory	JAX: 024671
Mouse: global <i>Tmbim1</i> KO mice	RIKEN BioResource Center	RBRC01773
Oligonucleotides		
The PCR primer for detection of recombination of <i>Tmbim1</i> -flox sites	Zhao et al., 2017	<i>Tmbim1</i> -P1 and <i>Tmbim1</i> -P2
The target sequence for the shRNA, see Table S2	This Paper	N/A
Primers used for lentivirus vectors and plasmids construction, see Table S3	This Paper	N/A
Primers for qPCR, see Table S4	This Paper	N/A
Recombinant DNA		
pHAGE_puro	Lu et al., 2018	Addgene Plasmid #118692
pLKO.1-TRC cloning vector	Moffat et al., 2006	Addgene Plasmid #10878
pMD2.G	Addgene	Addgene Plasmid #12259
psPAX2	Addgene	Addgene Plasmid #12260
Software and algorithms		
Leica Application Suite X (v4.3)	Leica Microsystems	https://www.leica-microsystems.com/products/microscope-software/p/leica-las-x-ls/
Graphpad Prism 7	Graphpad	https://www.graphpad.com/
SPSS statistics v23	IBM Corporation	http://www.spss.com.hk/software/statistics/
ImageJ v1.52	Schneider et al., 2012	https://imagej.nih.gov/ij/
Image Lab Software	Bio-Rad	https://www.bio-rad.com/en-cn/product/image-lab-software
HISAT2 v2.1.0	Kim et al., 2019	https://github.com/topics/hisat2
SAMtools v1.4	Li et al., 2009	https://github.com/samtools/
StringTie v1.3.3b	Pertea et al., 2015	http://ccb.jhu.edu/software/stringtie/
DESeq2 v1.2.10	Love et al., 2014	http://bioconductor.org/packages/release/bioc/html/DESeq2.html
Limma R package v3.40.0	Ritchie et al., 2015	https://bioconductor.org/packages/release/bioc/html/limma.html
Metascape	Zhou et al., 2019	http://metascape.org
R v3.6.1	R Core Team. R Foundation for Statistical Computing.	https://www.r-project.org
Java GSEA platform v3.0	Subramanian et al., 2005	http://software.broadinstitute.org/gsea/index.jsp
GSVA R package	Hänelmann et al., 2013	http://www.bioconductor.org/packages/release/bioc/html/GSVA.html
MASCOT engine v2.2	Matrix Science	http://www.matrixscience.com/
Cytoscape	Shannon et al., 2003	https://cytoscape.org/
Other		
Mouse high fat diet	Huafukang Bioscience	Cat#H10060
Mouse normal chow	Xietong	Cat#1010009
70 µm mesh filter	Falcon	Cat#352350
0.45 µm filter	Millipore	Cat#SLHV033RB
PVDF membrane	Millipore	Cat#IPVH00010

RESOURCE AVAILABILITY

Lead contact

Further information and requests for resources and reagents should be directed to and will be fulfilled by the Lead Contact, Hongliang Li (lihl@whu.edu.cn).

Materials availability

There are no restrictions to the availability of all materials mentioned in the manuscript.

Data and code availability

The RNA sequencing data generated in this study are available in the National Center for Biotechnology Information (NCBI) Sequence Read Archive (SRA) database. The accession numbers for the data reported in this paper are: PRJNA728240, PRJNA728494, PRJNA728533, PRJNA728546, PRJNA728526, PRJNA728551.

EXPERIMENTAL MODEL AND SUBJECT DETAILS

Animals

Tmbim1-Flox and CAG-loxP-CAT-loxP-*Tmbim1* mice were generated in our previous work (Zhao et al., 2017). AP-specific *Tmbim1* KO (*Tmbim1*-APKO) mice were generated by mating *Tmbim1*-Flox mice with *PdgfR α* -Cre mice (013148, Jackson Laboratory). AP-specific *Tmbim1* transgenic (*Tmbim1*-APTg) mice were generated by mating CAG-loxP-CAT-loxP-*Tmbim1* mice with *PdgfR α* -Cre mice. AP-specific *Ppar γ* KO (*Ppar γ* -APKO) mice were generated by mating *Ppar γ* -Flox mice (004584, Jackson Laboratory) with *PdgfR α* -Cre mice. AP-specific *Ppar γ* heterozygous KO (*Ppar γ* ^{f/+}-APKO) mice were generated by mating *Ppar γ* -Flox/+ mice with *PdgfR α* -Cre mice. AP-specific *Tmbim1* KO *Ppar γ* heterozygous KO mice (*Tmbim1*/*Ppar γ* ^{f/+}-APKO) were generated by mating *Tmbim1*-Flox; *Ppar γ* -Flox/+ mice with *PdgfR α* -Cre mice. Inducible adipocyte-specific *Tmbim1* KO (*Tmbim1*-iAKO) mice were generated by mating *Tmbim1*-Flox mice with *Adipoq*-CreER mice (024671, Jackson Laboratory). For the *Adipoq*-CreER experiments, 8-week-old male mice were given daily intraperitoneal injections of 100 mg per kg body weight (mg/kg) tamoxifen (T5648, Sigma-Aldrich) in corn oil (C116023, Aladdin, Shanghai, China) for 5 days and then allowed to recover for one week. *Tmbim1*-APKO mice reproduced normally and were born in normal Mendelian proportions. *Tmbim1*-APKO mice developed as normally as wildtype control mice and did not suffer from any spontaneous abnormalities when fed a NCD.

All animal protocols were approved by the Institutional Animal Care and Use Committee of the Center for Animal Experiments of Wuhan University and the Animal Care and Use Committee of Renmin Hospital of Wuhan University. The animals received humane care according to the Guide for the Care and Use of Laboratory Animals published by the National Academy of Sciences and the National Institutes of Health. Mice were housed in a temperature-controlled environment ($23 \pm 2^\circ\text{C}$) and relative humidity kept at 50 to 65% under a 12 h/12 h light/dark cycle with free access to food and water. Animals were housed strictly inbred in pathogen-free individually ventilated cage in our animal facility. The animals were housed at 3-5 mice per cage. Except for obesity, the mice were in generally good health. Eight-week-old male mice were fed a HFD (H10060, Huafukang Bioscience, Beijing, China) for 12 weeks. Mice that were fed a NCD (1010009, Xietong, Jiangsu, China) served as controls. For the *Adipoq*-CreER mice, HFD feeding started at the age of 10 weeks after tamoxifen injection and recovery. Fasting blood glucose levels were determined with a glucometer (One Touch Ultra Easy, Life Scan) after 6 h of fasting. For the GTTs and ITTs, the mice were intraperitoneally injected with 1 g per kg body weight (g/kg) glucose and 0.75 U/kg insulin after 6 h of fasting, respectively. The blood glucose levels were measured at 0, 15, 30, 60 and 120 min after injection. Serum insulin (CEA448Mu), leptin (SEA084Mu) and adiponectin (SEA605Mu) levels were measured with ELISA kits (Cloud-Clone, Wuhan, China). Serum TG (290-63701) and FFA (294-63601) levels were measured enzymatically using kits from WAKO Chemicals.

Cell lines and treatment

All cells were grown at 37°C in a 5% CO_2 humid atmosphere. HEK293T cells (GNHu17, Cell Bank of Type Culture Collection of the Chinese Academy of Sciences, Shanghai, China; sex unknown) were maintained in DMEM (8120268, Thermo Fisher Scientific) containing 10% FBS (10099141C, Gibco), and 3T3-L1 preadipocytes (CL-173, ATCC; sex unknown) were maintained in DMEM containing 10% NBCS (22011-8612, Every Green, Zhejiang, China). For transfection, HEK293T cells were transfected with indicated plasmids by polyethyleneimine (23966, Polysciences) method. When indicated, the cells were treated with cycloheximide (100 μM) (2112, Cell Signaling Technology), MG132 (10 μM) (S1748, Beyotime, Shanghai, China) or chloroquine (50 μM) (C6628, Sigma-Aldrich). All culture media were supplemented with 1% penicillin/streptomycin (PS) (15140-122, Gibco).

Primary cell isolation

MEFs (sex mixed) were isolated from embryonic day 14.5 embryos of WT and global *Tmbim1* KO (RBRC01773, RIKEN BioResource Center) mice, cultured in DMEM supplemented with 10% FBS and assayed at passages 3–6. SVFs and mature adipocytes were isolated as described (Church et al., 2014). Briefly, WAT from male mice was weighed, rinsed three times in PBS with 1% PS, and then minced and digested in 0.8 mg ml^{-1} collagenase type 2 (C6885, Sigma-Aldrich) in digestion buffer (0.4 g l^{-1} KCl, 0.06 g l^{-1} KH_2PO_4 , 8 g l^{-1} NaCl, 0.09 g l^{-1} $\text{Na}_2\text{HPO}_4 \cdot 7\text{H}_2\text{O}$, 1 g l^{-1} glucose, 1.2 mM CaCl_2 , 1 mM MgCl_2 , 0.8 mM ZnCl_2 , 3% BSA) for 75 min at 37°C in a shaking water bath (120–140 rpm) including vigorous shaking by hand (for 10–20 s) after 60 min of incubation. Floating adipocytes were separated from the SVF by centrifugation at 300 g for 3 min. The floating mature adipocytes were collected, and the SVF pellet was resuspended in digestion buffer, filtered through sterile 70 μm mesh filters (352350, Falcon), and then cultured in DMEM/F12 (C11330500BT, Gibco) with 10% FBS or proceeding with AP isolation. APs were then isolated as per the manufacturer's protocol (130-106-639, Miltenyi) using negative selection of CD45 and CD31 followed by positive selection for SCA-1. Briefly, SVF suspensions were incubated with the Non-Adipocyte Progenitor Depletion Cocktail, washed and passed over a lineage depletion column.

The retained cells were Lin⁺ cells (CD45- and CD31-positive) and were eluted. The flowthrough was collected, washed, and incubated with the Adipocyte Progenitor Isolation Cocktail. The cells were then washed and passed over a lineage selection column. The retained cells were APs and were eluted.

METHOD DETAILS

Adipocyte differentiation

The day when cells reached confluence was designated as day -2. For 3T3-L1 cells, two days after confluence (day 0), they were induced to differentiate with DMEM containing 10% FBS and 1 µg ml⁻¹ insulin (I6634, Sigma-Aldrich), 0.5 mM 1-methyl-3-isobutyl-xanthine (IBMX) (I7018, Sigma-Aldrich), 0.25 µM dexamethasone (D4902, Sigma-Aldrich) and 2 µM rosiglitazone (R2408, Sigma-Aldrich) until day 2. The cells were then cultured with DMEM supplemented with 10% FBS and insulin (1 µg ml⁻¹) for 2 days, after which they were cultured with DMEM containing 10% FBS; the medium was changed every other day. For MEFs and IngWAT-isolated SVFs, primary cells were first cultured to confluence in DMEM/F12 medium containing 10% FBS and 1% PS and then induced with a differentiation cocktail consisting of 5 µg ml⁻¹ insulin, 0.5 mM IBMX, 1 µM dexamethasone and 2 µM rosiglitazone in DMEM/F12 supplemented with 10% FBS and 1% PS. After 2 days, the medium was replaced with DMEM/F12 containing 10% FBS, 1% PS, 5 µg ml⁻¹ insulin and 2 µM rosiglitazone every other day. Lipid droplet formation was visualized using BODIPY 493/503 (D3922, Thermo Fisher Scientific) or Oil Red O (O1391, Sigma-Aldrich) staining. Adipocytes were firstly fixed in 3.7% formaldehyde solution (F8775, Sigma-Aldrich) for 15 min. For BODIPY 493/503, fixed cells were incubated at 0.1 µg ml⁻¹ for 10 min and counterstained with DAPI (0100-20, SouthernBiotech) before visualization with a confocal microscope (TCS SP8, LEICA, Wetzler, Germany) and quantification using Leica Application Suite X software. BODIPY fluorescence intensities were normalized by cell counts. The Oil Red O staining was performed as previously described (Liu et al., 2020), fixed cells were incubated in 60% isopropanol for 5 min, and stained with Oil Red O solution for 15 min.

Construction of the lentivirus vector

For stable gene overexpression, the *Tmbim1* (WT or PSAP motif deletion), *Pparγ* and *Nedd4* gene was cloned into pHAGE-puro vector (118692, Addgene) (Lu et al., 2018) with Flag or HA tags. The N-terminal Cherry tagged *Tmbim1* or C-terminal GFP tagged *Nedd4* gene was cloned into pHAGE-puro vector. For stable RNA interference, shRNAs were cloned into the pLKO.1 lentiviral vector (10878, Addgene) (Moffat et al., 2006). A shRNA that targeted GFP was used as the control. Recombinant lentiviruses were produced by co-transfected HEK293T cells with the lentiviral expression and packaging plasmids psPAX2 (12260, Addgene) and pMD2.G (12259, Addgene), respectively. The virus-containing supernatant was harvested at 48 h and 72 h after transfection, and the virus was filtered through a 0.45 µm filter (SLHV033RB, Millipore) before infection. The target sequences for the shRNAs are shown in Table S2.

Plasmid construction

Plasmid encoding Flag-Tmbim1 were obtained by cloning the cDNA encoding *Tmbim1* into the CAG-Flag vector. Plasmids encoding full-length or truncated Flag-Cherry-Tmbim1 or HA-Nedd4 were obtained by cloning the indicated *Tmbim1* or *Nedd4* cDNAs into the pcDNA3.1-Flag-Cherry vector or pcDNA3.1-HA vector. Plasmid encoding full-length HA-His-Nedd4 was obtained by cloning His tagged *Nedd4* cDNAs into the pcDNA3.1-HA vector. Plasmid encoding HA-His-Nedd4 (C854S) was generated by site-directed mutagenesis. The primers used for lentivirus vectors and plasmids construction are listed in Table S3.

RNA isolation and qPCR

Total RNA was extracted with TRI Reagent (T9424, Sigma-Aldrich) and then reverse-transcribed into cDNA by using a Transcriptor First-Strand cDNA Synthesis Kit (04896866001, Roche) according to the manufacturer's instructions. The real-time PCR system (LightCycler480 Instrument II, Roche Diagnostics Inc., Basel, BS, Switzerland) and SYBR Green (04887352001, Roche) were used to quantify the PCR amplification products. The mRNA expression levels of the target genes were normalized to that of 18S rRNA. The primer sequences for qPCR are shown in Table S4.

Western blotting

Total protein samples were isolated by treating tissue or cell samples with RIPA lysis buffer (65 mM Tris-HCl, pH 7.5, 150 mM NaCl, 1 mM EDTA, 1% Nonidet P-40, 0.5% sodium deoxycholate, 0.1% SDS, protease inhibitor cocktail tablets (04693132001, Roche) and phosphatase inhibitor tablets (4906837001, Roche)). The BCA Protein Assay Kit (23225, Thermo Fisher Scientific) was used to measure protein concentrations. Proteins were separated using 10% SDS-PAGE gels and then transferred to PVDF membranes (IPVH00010, Millipore). After the membranes were blocked in 5% skim milk, they were incubated overnight at 4°C with primary antibodies and then for 1 h at room temperature with the corresponding secondary antibodies. A ChemiDoc MP Imaging System (Bio-Rad) was used for signal detection. Protein expression levels were quantified using Image Lab software and normalized to the levels of β-Actin, which was used as a loading control.

Histological analyses and adipocyte size

WAT was fixed and embedded in paraffin and then sectioned and stained with H&E. After H&E staining, the histopathological images were obtained with digital pathology scanner (Aperio Versa 200, LEICA, Buffalo Grove, USA). Adipocyte areas was measured

manually using ImageJ software ([Schneider et al., 2012](#)) for at least 100 adipocytes for each animal. The frequency distributions of the adipocyte size were determined as previously described ([Parlee et al., 2014](#)). Briefly, any objects that fall below an area of $350 \mu\text{m}^2$ were firstly removed as these cells may be a mixture of adipocytes and stromal vascular cells. The frequency was calculated using the frequency function in Excel (= frequency (data_array, bins_array)) with array bins in $1000 \mu\text{m}^2$ increments. The number of total adipocytes within the distribution was subsequently calculated and used to convert the frequency to a percentage of total adipocytes counted. Immunohistochemistry were performed on paraffin embedded WAT sections. For antigen retrieval, samples were heated in a pressure cooker for 20 min in pH 9.0 EDTA buffer. After cooling, samples were placed in 3% H₂O₂ for 20 min to quench endogenous peroxide activity. After washing with PBS, slides were blocked with 10% BSA for 10 min. Sections were incubated with the F4/80 primary antibody (MCA497, Bio-Rad) overnight at 4°C, washed with PBS buffer for 3 times (3 min/wash) and then incubated with enhanced enzyme-labeled goat anti-rat IgG (PV-9004, ZSGB-Bio, China) for 1 h at room temperature. The sections were visualized with DAB (ZLI-9018; ZSGB-Bio, China) and counterstained with hematoxylin.

Immunoprecipitation assay

IP assays were performed as previously described ([Zhao et al., 2017](#)). Briefly, cells were transfected for 24 h with the indicated plasmids, lysed in ice-cold immunoprecipitation (IP) buffer (50 mM Tris-HCl, pH 8.0, 150 mM NaCl, 1 mM EDTA, 1% Triton X-100 and 0.5% sodium deoxycholate) containing protease inhibitor cocktail tablets (04693132001, Roche) and centrifuged at 13000 g for 15 min. The cell lysates were then incubated with the indicated antibodies and Protein G-agarose (11719416001, Roche) overnight at 4°C followed by washing in cold IP buffer. The normal mouse IgG (sc-2025, Santa Cruz Biotechnology) was used as negative control. The immunocomplexes were collected and subjected to immunoblotting using the indicated primary antibodies and corresponding secondary antibodies. Clean-Blot IP Detection Reagent (21230, Thermo Fisher Scientific) was used to prevent interference from denatured IP antibody fragments.

In vivo ubiquitination assays

The *in vivo* ubiquitination assay was performed as previously described ([Zhao et al., 2017](#)). Briefly, cells (from a well of a 6-well plate) were washed with PBS, pelleted and lysed in 250 µl of lysis buffer (50 mM Na₂HPO₄, pH 8.0, 300 mM NaCl, 1% Triton X-100 and protease inhibitor cocktail tablets). The lysates were centrifuged (13,000 g for 15 min at 4°C), and the supernatants were diluted tenfold with urea buffer (8 M urea, 50 mM Na₂HPO₄, pH 8.0, 300 mM NaCl, 10 mM imidazole, 0.2% Triton X-100 and protease inhibitor cocktail tablets) before the addition of 20 µl of Ni-NTA agarose (30210, Qiagen). After the mixture was rotated at 4°C for 2.5 h, the beads were washed twice with 1 ml of urea buffer followed by two washes with 1 ml of urea-TI buffer (urea/TI volume ratio 1:3; TI buffer: 20 mM Tris-HCl, pH 6.8, 300 mM NaCl, 0.2% Triton X-100, 20 mM imidazole and 0.2% SDS). Then, the beads were washed twice with TI buffer followed by two washes with TI high salt buffer (TI buffer with 1 M NaCl). After another wash with TI buffer, the supernatant was completely removed with thin micropipette tips. The proteins were released from the beads by boiling for 10 min in 40 µl of 2× SDS-PAGE sample buffer containing 200 mM imidazole.

Cellular localization

First, 3T3-L1 cells were coinjected with Cherry-Tmbim1-expressing and Nedd4-GFP-expressing lentiviruses. After 48 h, the cells were fixed with 3.7% formaldehyde solution and stained with DAPI. Images were acquired using a confocal microscope.

RNA-Seq

The RNA-Seq was performed as previously described ([Jian et al., 2020](#)). Briefly, total RNA was extracted using TRI Reagent (T9424, Sigma-Aldrich) and the quality of the extracted total RNA samples was examined with RNA 6000 Nano kit (5067-1511, Agilent). The MGIEasy RNA Library Prep Kit (1000006384, MGI Tech, Shenzhen, China) was used for library preparation according to the manufacturer's instructions. Briefly, after mRNA enrichment, the samples were incubated with fragmentation buffer to obtain a target insert fragment size of ~150 bp. Then, the fragments were reverse-transcribed into cDNA. After repair and A-tailing, the double-stranded cDNA products were ligated with adaptors and subjected to PCR amplification (95°C for 30 s, 56°C for 30 s, and 72°C for 60 s; 14 cycles). The PCR products were cleaned using DNA Clean Beads. Then quality control of the purified PCR products was carried out with an DNA 1000 Kit (5067-1504, Agilent). PCR products at ~230 bp in size were subjected to multiple-sample pooling, amplification, and digestion to obtain the libraries. Gene expression analysis was performed by mRNA sequencing on a BGISEQ-500 instrument (MGI Tech) with a single-end 50 bp module.

Digital gene expression

The reads were mapped to Ensembl mouse (mm10/GRCm38) reference genomes by HISAT2 software version 2.1.0 ([Kim et al., 2019](#)) and Binary Alignment Map (BAM) files were generated to store the alignments by SAMtools ([Li et al., 2009](#)). StringTie ([Pertea et al., 2015](#)) was used to calculate Fragments Per Kilobase of exon model per Million mapped fragments (FPKM) value. Differential genes expression analysis were computed by DESeq2 ([Love et al., 2014](#)). Differential expressed genes (DEGs) were identified with two standards: (1) the fold change larger than 1.5 and (2) the corresponding adjusted P values less than 0.05.

Microarray data analysis

The microarray data of GSE41578 was download from GEO database ([Galhardo et al., 2014](#)). Differential expressed genes (DEGs) were identified by Limma R package ([Ritchie et al., 2015](#)) with two standards: (1) the fold change larger than 1.5 and (2) the corresponding q values less than 0.05.

Gene expression patterns classification

Union of $|\log_2\text{Foldchange}|$ top 500 DEGs in each pairwise comparisons of any two of the three time points in 3T3-L1 and SGSB cell lines were used for gene expression patterns classification. The classification of the genes was based on gene expression fold-changes between two consecutive stages. A positive $\log_2(\text{Foldchange})$ indicates that the gene is upregulated, and a negative $\log_2(-\text{Foldchange})$ indicates that the gene is downregulated.

Functional enrichment

The functional enrichment of genes with consistent expression trends in 3T3-L1 and SGSB cell lines was using “Metascape” online tool ([Zhou et al., 2019](#)) based on Gene Ontology (GO) biological process (BP).

KEGG pathway enrichment analysis

A KEGG pathway enrichment analysis of all differently expressed genes was performed using Fisher’s exact test with our in-house R script, and the KEGG pathway annotations of all genes in the selected genome were download from KEGG database. The pathway with a P value < 0.05 was defined as significantly enriched pathway.

Gene set enrichment analysis

Each GO biological process (BP)/KEGG pathway term and involved genes were defined as gene sets, and GSEA was implemented on the Java GSEA platform ([Subramanian et al., 2005](#)) with the ‘Signal2Noise’ metric to generate a ranked list and a ‘gene set’ permutation type. Gene sets with FDR values < 0.25 were considered statistically significant. The expression levels of leading genes in the enriched pathways of GSEA was exhibited by heat map using the “pheatmap” package in R. The average gene expression levels of biological replicates were normalized using the Z-score transformation method. The color key of all heat maps is the Z-score normalized FPKM (Fragments Per Kilobase of exon model per Million mapped fragments).

Gene set variation analysis

Gene set variation analysis was carried out to estimate sample-wise KEGG pathway activity variation using the GSVA R package ([Hänelmann et al., 2013](#)). For each KEGG pathway with at least ten genes, the gene expression matrix was subjected to calculate the single sample GSVA scores.

Mass spectrometry analysis

3T3-L1 cells were infected with lentivirus encoding Flag-Cherry-TMBIM1 or Flag-Cherry then induced adipocyte differentiation for 4 days. The lysis of cells and immunoprecipitation of TMBIM1 and its interacting proteins were performed as described above in the IP assay. The IP sample were subjected to SDS-PAGE and run for approximate 1 cm of migration of bromophenol blue dye. The gels were excised and reduced using 10 mM DTT/100 mM NH₄HCO₃ and alkylated using 200 mM IAA/100 mM NH₄HCO₃ in the dark at room temperature for 30 min. In-gel digestion was then conducted overnight in 12.5 ng μl^{-1} trypsin in 25 mM NH₄HCO₃. The peptides were extracted three times with 60% ACN/0.1% TFA. The extracts were pooled and dried completely by a vacuum centrifuge. To perform the LC-MS/MS analysis, the peptide mixture was loaded onto a reverse phase trap column (Acclaim PepMap100, 100 $\mu\text{m}^2\text{cm}$, nanoViper C18, Thermo Fisher Scientific) connected to the C18-reversed phase analytical column (Easy Column, 10 cm long, 75 μm inner diameter, 3 μm resin, Thermo Fisher Scientific) in buffer A (0.1% Formic acid) and separated with a linear gradient of buffer B (84% acetonitrile and 0.1% Formic acid) at a flow rate of 300 nL/min controlled by IntelliFlow technology. A Q-Exactive mass spectrometer (Thermo Fisher Scientific) was coupled to Easy nLC (Proxeon Biosystems). The mass spectrometer was operated in positive ion mode. MS data was acquired using a data-dependent top10 method dynamically choosing the most abundant precursor ions from the survey scan (300–1800 m/z) for HCD fragmentation. Automatic gain control (AGC) target was set to 3e6, and maximum inject time to 10 ms. Dynamic exclusion duration was 40.0 s. Survey scans were acquired at a resolution of 70000 at m/z 200 and resolution for HCD spectra was set to 17500 at m/z 200, and isolation width was 2 m/z. Normalized collision energy was 30 eV and the underfill ratio, which specifies the minimum percentage of the target value likely to be reached at maximum fill time, was defined as 0.1%. The instrument was run with peptide recognition mode enabled. MS/MS spectra were searched using MASCOT engine against a nonredundant International Protein Index arabidopsis sequence database v3.85 (released at September 2011; 39679 sequences) from the European Bioinformatics Institute (<http://www.ebi.ac.uk/>). The criteria of the candidate proteins selection for further study are as follows: (1) the proteins should be present in the Flag-Cherry-TMBIM1 group but be diminished in the Flag-Cherry group; (2) number of unique peptides ≥ 1 . The protein-protein interaction network was constructed by Cytoscape ([Shannon et al., 2003](#)). The proteins that were found to interact with TMBIM1 are shown in [Table S1](#).

QUANTIFICATION AND STATISTICAL ANALYSIS

All data were analyzed in SPSS software and are expressed as the mean \pm SEM. Normal distribution of populations at the 0.05 level was calculated using the Shapiro-Wilk normality test. A two-tailed Student's t-test was used to compare differences between two groups and one-way ANOVA was performed for multiple comparisons, followed by Bonferroni analysis. A two-way ANOVA was applied for multiple comparisons with two independent variables. The statistical methods of each experiment and all *P* values and *n* are indicated in the figure legends. No blinding experiments were performed. Mice were randomly allocated to groups. Sample size was estimated by pilot experiments that showed trends of effects as well as previous experience based on similar experiments. No data were excluded when performing the statistical analysis. Data were judged to be statistically significant when *P* < 0.05 (**P* < 0.05, ***P* < 0.01).